EVALUATION OF SPATIAL RESOLUTION AND THE NON-LINEARITY ANALYSIS FOR 3-D METROLOGY

by

Swati Jain

A dissertation submitted to the faculty of
The University of North Carolina at Charlotte
in partial fulfillment of the requirements
for the degree of Doctor of Philosophy in
Optical Science and Engineering

Charlotte

2021

Approved by:

_____
Dr. Angela Davies Allen

_____
Dr. Glenn Boreman

_____
Dr. Christopher Evans

_____
Dr. Greg Gbur

ABSTRACT

SWATI JAIN. Evaluation of Spatial Resolution and the Non-Linearity Analysis for 3-D Metrology. (Under the direction of DR. ANGELA D. ALLEN)

Structured light systems (SLS) have become increasingly important for three-dimensional shape measurements. A quantitative evaluation of the spatial resolution is also becoming increasingly important. The spatial frequency response of the instrument is a reasonable metric for resolution and is commonly referred to as the instrument transfer function (ITF). We used the ITF to determine the capability of a commercial SLS the EinScan-pro using a step artifact. The ITF is similar to the modulation transfer function (MTF) of an imaging system, which describes how well the system images an object as a function of spatial frequency. Similarly, ITF describes the instrument response to the spatial frequency on the surface to be measured. Many optical measurement instruments use a camera for data acquisition and the optical transfer function will necessarily impose a limit on the instrument resolution. The ITF and the MTF metrics rely on the linearity of the measurement. Only a liner and shift-invariant system can be used to uniquely define ITF/MTF. In this dissertation, we describe the use of the step artifact to determine the spatial resolution of a commercial SLS the EinScan-Pro. We check the use of the ITF over the MTF of the imaging system. We present a methodology to check the combined uncertainty for the ITF measurements including a method to check the applicability of the step artifact for the ITF measurements, the impact of the use of step artifact with different surface finishes, and the effect of the tilt and disposition of the artifact during the measurement. We also, present the use of the bispectrum for the non-linearity check of any kind of measurement which is applicable for both ITF/MTF measurements.

ACKNOWLEDGEMENTS

Foremost, I would like to express my sincere gratitude to my advisor Angela Davies Allen for the continuous support throughout my Ph.D. study and research. I thank her for her patience, motivation, enthusiasm, and immense knowledge. Her guidance helped me in all the time of research and writing of this thesis. I could not have imagined having a better advisor and mentor for my Ph.D. study.

Besides my advisor, I would like to thank the rest of my thesis committee members: Dr. Glenn Boreman, Dr. Greg Gbur, and Dr. Christopher Evans for their encouragement, suggestions, and insightful comments.

My sincere thanks also go to Dr. Joshua Tarbutton for allowing us to use his instrument through the study. I would like to express sincere gratitude to Dr. Faramarz Farahi for guiding and helping me with the bispectrum study and sharing his knowledge. I offer my special thanks to Dr. Bin Zhang for his assistance at an early stage of this project.

I would like to extend my sincere thanks to Scott Williams, Lou, Jeffery Thousand, and Micahel Dhooghe for their assistance with the experimental setup. In addition, I would like to thank Greg Caskey for his assistance with scanning white light interferometer measurements.

Last but not the least, I would like to thank my husband, my family, and friends as a whole for their continuous support and understanding when undertaking my research and writing my thesis.

TABLE OF CONTENTS

LIST OF FIGURES viii

LIST OF ABBREVIATIONS xii

INTRODUCTION 1

Chapter 1. EVALUATION OF THE SPATIAL FREQUENCY RESPONSE AND THE UNCERTAINTY FOR A COMMERCIAL STRUCTURED LIGHT SYSTEM 5

ABSTRACT 5

1.1 Introduction 5

1.2 Theory 7

1.2.1 Definition of ITF 7

1.2.2 Method of Calculating ITF 8

1.3 Artifacts for ITF Measurement 9

1.4 Einscan-pro 3d scanner (A commercial structured light system) 10

1.5 Measurement object: step artifact 11

1.6 Data processing for The ITF measurement 14

1.6.1 Coordinate Transformation 14

1.6.2 Average step profile to reduce measurement noise 15

1.6.3 Calculation of ITF 17

1.7 Uncertainty Analysis for The ITF measurement 18

1.8 ITF as a function of step orientation 19

1.9 ITF as a function of WORKING distance 20

1.10 MTF Vs ITF 21

1.11 Conclusion 23

ACKNOWLEDGEMENTS 24

REFERENCES 25

Chapter 2. ESTIMATING UNCERTAINTY FOR THE INSTRUMENT TRANSFER FUNCTION MEASUREMENT OF 3D SCANNERS 28

2.1 Introduction 28

2.2 Theory 29

2.3 Data Processing 34

2.4 Uncertainty Analysis 35

2.4.1 Model Assumption 36

2.4.2 Measurement conditions 42

2.4.3 Environment factors 47

2.4.4 Coordinate Transformation 47

2.4.5 Calculation of average step profile 48

2.4.6 Repeatability 50

2.5 Measured ITF 50

2.6 Conclusion 52

REFERENCES 54

Chapter 3.DETERMINATION OF NON-LINEARITY FOR 3D MEASUREMENTS .. 58

ABSTRACT 58

3.1 Introduction 58

3.2 Coherence Function..... 61

3.2.1 Use of the coherence function for determination of non-linearity with sinusoidal waves..... 62

3.2.2 Failure of the coherence function for determination of non-linearity with a step artifact 64

3.3 The Bispectrum 65

3.3.1 Use of the bispectrum for determination of non-linearity with sinusoidal waves 67

3.3.2 Use of the bispectrum to determine the non-linearity with a step artifact..... 69

3.4 Conclusion..... 74

REFERENCES 76

CONCLUSION 82

REFERENCES 85

LIST OF FIGURES

Fig. 1-1. EinScan-Pro 3D Scanner. 11

Fig. 1-2. SWLI measurement of top surfaces of the step artifact: (a) top surface, and (b) line profile along the line shown in (a). 13

Fig. 1-3. Experimental Set-up for ITF Measurement. 14

Fig. 1-4. Measured Point Cloud Data. 14

Fig. 1-5. (a) Define Local Coordinate System with a plane fit to lower terrace, (b) Data in Local Coordinate System, (c) Top View of Data in Local Coordinate System and (d) Presence of high-frequency shoulder. 15

Fig. 1-6. (a) Resampling of higher density 1-D step profile, and (b) Average step profile. 16

Fig. 1-7. Sigmoid Function fit to the measured step profile. 17

Fig. 1-8. (a) LSF by taking derivative of Sigmoid fit step profile, and (b) ITF estimation by taking Fourier transform of LSF. 17

Fig. 1-9. The best estimate of ITF along with uncertainty at 380mm. 19

Fig. 1-10. ITF dependence on step orientation. (a) No. of data points as a function of bin no. for negative angles and (b) Slope of the step transition as a function of angle for all tilt angles. 20

Fig. 1-11. The ITF cutoff frequency is a function of distance. 21

Fig. 1-12. An image of the slanted knife edge for the MTF measurement. 22

Fig. 1-13. Comparison of ITF and MTF of Camera-1 and Camera-2. (a) At 350mm, (b) at 390mm (MTF best Focus), and (c) At 450mm. 23

Fig. 1-14. Comparison of ITF and MTF's as a function of distance. 23

Fig. 2-1. Validity limit of a step artifact. 32

Fig. 2-2. (a) Photograph of the step artifact used for the ITF measurements and (b) cross-section schematic of the sample..... 34

Fig. 2-3. Experimental set-up for ITF measurement..... 35

Fig. 2-4. The fishbone diagram..... 36

Fig. 2-5. (a) Measurement condition for the top corner of the step artifact, (b) The roundness of the bottom corner is undercut. and (c) Measured radius of the top corner.. 38

Fig. 2-6. (a) The frequency response of the estimated step profile by measured radius and with 10 µm corner radius step profile is far beyond the best possible frequency response when limited by instrument LSF. (b) Two steps created using. (1) the artifact step radius (10 µm) and (2) the best possible step profile when a line-spacing-generated LSF is used. 39

Fig. 2-7. Tilt condition of the step artifact about the measurement axis. 40

Fig. 2-8. (a) Tilt in the negative direction from the measurement axis leads to shadowing and appears as data drop out in the step profile. (b) Tilt in the positive direction leads to an undercut step profile..... 41

Fig. 2-9. (a) Incident light on a specular edge (black profile) is reflected, resulting in the mirror image of the diffuse surface to the left (dashed gray profile). (b) An undercut step profile results after completing the coordinate transformation data processing step..... 42

Fig. 2-10. The 50% cutoff value of the ITF as a function of the artifact position along the measurement axis shows the best resolution is at 380mm..... 43

Fig. 2-11. (a) Location of artifact around the center of the FOV at 400 mm and (b) The ITF at different positions around the center of the FOV at best focus. 44

Fig. 2-12. (a) The simulated step profiles at zero and +15^{o} show how the apparent corner curvature varies with misalignment angle, and (b) the ITF results show the ITF is lowest at 0^{o} and highest at 15^{o} 46

Fig. 2-13. The ITF at different rotation orientations at the 400 mm in the middle of the FOV 47

Fig. 2-14. Slope comparison approach for the uncertainty calculations due to the choice of the process parameter (angle calculation) 49

Fig. 2-15. The ITF for different resampling intervals 50

Fig. 2-16. The final estimate of the ITF with the uncertainty 52

Fig. 3-1. (a) An example of a linear system and (b) an example of a non-linear system. 59

Fig. 3-2. Input and output sinusoidal signals with input having the frequencies of 25mm^{-1} and 100mm^{-1} and the output signal contains additional harmonics of sum frequency 125mm^{-1}, the difference of frequency 75mm^{-1} and double frequencies of 50mm^{-1} and 200mm^{-1} 63

Figure 3-3. The coherence function calculated for a sinewave shows the presence of the harmonics. 64

Fig. 3-4. (a) Input and a non-linear output, and (b) The coherence function for a step function is one over the whole frequency range 65

Fig. 3-5. (a) Two signals before adding noise having different frequencies of 25mm^{-1} and 50 mm^{-1}, and (b) Total Signal sum of the two signals in (a) plus a random noise with a standard deviation of 20. 68

Fig. 3-6. The Fourier transform of sinewave in Fig. 1(b) shows the difficulty to recognize the presence of inherent frequency in the signal due to noise. 68

Fig. 3-7. A line profile along the line f1=f2 (along diagonal), and the bispectrum show a strong peak at f1=25mm^{-1}, confirming the existence of 2f1=50mm^{-1} in the signal. 69

Fig. 3-8. A linear camera model is shown in gray, and a non-linearity response curve in black, showing the linear response at low intensity and the nonlinear response with increasing intensity input due to camera saturation. The fir to the non-linear response curve is a 4th order degree polynomial. 71

Fig. 3-9. A comparison of linear (gray curve) and non-linear (black curve) steps. 72

Fig. 3-10. The normalized bispectrum of the linear step. 72

Fig. 3-11. A line profile along diagonal showing the bispectrum of a non-linear step is higher than that of a linear step function. 73

Fig. 3-12. The subtraction of non-linear and linear bispectrum shows the presence of non-linearity. Inset shows the zoomed view from f=0 mm-1 to 100 mm-1 showing a significant sign of non-linearity. 73

Fig. 3-13. A line profile along diagonal showing the bispectrum of a non-linear step is higher than that of a linear step function when random noise is added, and the subtraction of non-linear and linear bispectrum when noise is added. The presence of non-linearity is still detectable. Inset shows the zoomed view from f=0 mm^{-1} to 100 mm^{-1} showing a significant sign of non-linearity. 74

LIST OF ABBREVIATIONS

SLS	structured light system
ESF	edge spread function
FFT	fast Fourier transform
ITF	instrument transfer function
MTF	modulation transfer function
OTF	optical transfer function
LSF	line spread function
PSF	point spread function
RMS	root mean square
FOV	field of view
FWHM	full width half maxima
CCD	charge coupled device
HOSA	higher order spectral analysis
HOS	higher order spectrum
BS	bispectrum

INTRODUCTION

In recent years, structured light systems (SLS) have become popular for acquiring 3D geometric measurements because they are non-contact and fast. The applications range from inspection of small-scale IC packages to large-volume metrology of power generators [1,2]. The advancement in several areas (such as cameras, computing power, processing hardware, projection, and illumination systems) enables higher density point cloud data, which can mislead the users in terms of the spatial resolution of the measurement. Therefore, there is a need to define and quantify the spatial resolution of these instruments. The conventional definition of spatial resolution is the ability of the instrument to detect two adjacent points [3]. According to Rayleigh, two points are said to be resolved if the center of the point spread function (PSF) of one point falls at the first zero of the PSF of the other point. This definition is reasonable for microscopic or biological imaging applications. For a surface or dimensional measurement, it is reasonable to define spatial resolution in terms of the spatial frequency response of the system. This is called the instrument transfer function (ITF) in the literature [3,4].

The ITF is defined as the response of the instrument to the spatial frequency content of the object [3,4] and provides a complete description of instrument performance over the full range of spatial frequencies. The spatial frequency at which the ITF falls to 50% is called the lateral period limit and is the measure of spatial resolution of the instrument as defined in ISO 25178-604 [3,9]. The ITF is similar to the modulation transfer function (MTF) of an imaging system, which describes how well the system images an object as a function of spatial frequency. Similarly, the ITF describes the instrument response to the

spatial frequency on the surface to be measured. Many optical measurement instruments use a camera for data acquisition and the optical transfer function will necessarily impose a limit on the instrument resolution. The study of the ITF for structured light systems (SLS) is relatively new with a few published studies [5-8]. Our first paper includes a methodology to estimate the ITF of a commercial SLS (the EinScan-Pro 3D Scanner) following the step-artifact approach and its uncertainty. The ITF dependence on the position in the measurement volume is also investigated. More interestingly, a comparison of the measured ITF and MTF of the instrument is also presented which shows that the ITF is higher than the MTF at distances shorter than best focus.

Our second paper extends this study and presents a complete survey of determining the uncertainty of the ITF measurements. Based on ISO standard the ITF predicts the 50% frequency cutoff 2.6 mm^{-1} which corresponds to a 50% cutoff wavelength of 0.38 mm which is approximately two times larger than the 0.16 mm point spacing, which would be a user's estimate of the resolution. The second paper includes several factors that must be considered carefully while measuring an instrument's ITF and processing the data. If care is taken with the alignment of the step artifact, the most important contributions to our uncertainty are the repeatability and the angle estimation to rotate back and align the measured step edge during data processing. Concerning alignment, the angle of the artifact to the projection axis (the angle of the normal vector of either terrace of the step artifact to the measurement axis) is important. A negative tilt angle leads to the shadowing effect which appears as data dropout. Tilt in the positive direction will cause an apparent undercut in the step profile in the case of the specular edge step artifact whereas a diffuse edge leads to an artificially improved ITF estimate. This is purely a geometric projection effect. The

sensitivity of the ITF to the step orientation of the artifact within the field of view was also discussed, and the ITF was found to be insensitive to this measurement condition. The choice of the resampling interval was also explored. In addition, the characterization and validation methods for the step artifact were discussed.

The modulation transfer function and the instrument transfer function are practical metrics to quantify the spatial frequency response of imaging systems and three-dimensional topographical measurements, respectively [4,5,9]. However, a frequency response based metric for the resolution relies on an assumption of measurement linearity. Without this assumption, the frequency response (and therefore resolution) becomes a function of the measured/imaged object itself and therefore cannot be universally quantified. Most 3D topography measurements show non-linear behavior particularly for high spatial frequency components in the limit in particular where the resolution metric is needed [3-4,9-15]. Therefore for a valid resolution characterization, investigation of the presence of non-linearity is also important. In our third paper, we present a general methodology of identifying non-linearity in a measurement that can be used for both imaging systems as well as 3D topography instruments.

A system is said to be linear if its response is the sum of the responses that each of the frequency component signals would produce individually, i.e., if two frequency components are present in an input signal, we can propagate them separately and add up the result [3,11]. For example, for a linear system, the output of a sinusoidal input would be sinusoidal with only a modified amplitude. However, a non-linear system will generate harmonics of a sinusoidal input, changing both the shape and the scale (e.g. reducing and flattening the peaks of the sinusoid). In general, surface topographic measurements are

non-linear, particularly for complex textures and high surface slopes, however, limits can be defined where measurements are approximately linear. These conditions depend on the physical principle of the measurement and the instrument classes. Our analysis method can be used to determine if the instrument is operating in a nonlinear limit and can be applied to any instrument, and for both ITF and MTF characterization.

Our third paper presents an analysis method to determine whether a measurement is approximately linear and applies to any optical topographic or optical imaging measurement. Our approach uses the coherence function calculation from the structure dynamics community for use with a sinusoidal-based artifact for the MTF/ITF measurement. The coherence function calculation does not work for a step artifact, however, which is commonly used in the MTF/ITF measurements. For a step-based artifact, we present the use of a higher-order spectral function - the bispectrum - for non-linearity detection. The bispectrum can also be used with discrete sinusoidal based artifacts.

Chapter 1. EVALUATION OF THE SPATIAL FREQUENCY RESPONSE AND THE UNCERTAINTY FOR A COMMERCIAL STRUCTURED LIGHT SYSTEM

ABSTRACT

Structured light systems (SLS) have become increasingly important for three-dimensional shape measurements. A quantitative evaluation of the spatial resolution is also becoming increasingly important. The spatial frequency response of the instrument is a reasonable metric for resolution and is commonly referred to as the instrument transfer function (ITF). In this paper, we present a methodology to estimate the ITF of a commercial SLS (the EinScan-Pro 3D Scanner) and its uncertainty. A measurement of a step artifact is used for the ITF estimation. We also discuss a method to check the validity of the artifact used for the measurement. The ITF dependence on step orientation and position in the measurement volume is also presented, in addition to a comparison between ITF and the modulation transfer function (MTF) for the cameras in the instrument.

1.1 Introduction

Structured light systems have become increasingly important in many manufacturing sectors [1,2]. The applications range from inspection of small-scale IC packages to large volume metrology of power generators [1,2]. The application growth is enabled by technology advances in several areas, such as high resolution, high sensitivity, megapixel cameras, computing power, processing hardware, digital projection system, and illumination systems[1]. These advances enable higher density point cloud data, which can mislead the user in terms of spatial resolution. Therefore, there is a need to define the spatial resolution of these instruments. The conventional definition of spatial resolution is the ability of the instrument to detect two adjacent points [3]. According to Rayleigh, two points are said to be resolved if the center of the point spread function (PSF) of one point

falls at the first zero of the PSF of the other point. This definition is reasonable for microscopic or biological imaging applications. For a surface or object dimensional measurement, it is reasonable to define spatial resolution in terms of the spatial frequency response of the system. This is called the instrument transfer function (ITF) in the literature [3,4].

The ITF is defined as the response of the instrument to the spatial frequency content of the object [3,4] and provides a complete description of instrument performance over the full range of spatial frequencies. The spatial frequency at which the ITF falls to 50% is called the lateral period limit and is the measure of spatial resolution of the instrument (ISO 25178-604) [3,9]. The study of the ITF for structured light systems (SLS) is relatively new with a few published studies [5-8]. The ITF dependence on experimental factors for commercial systems has not been investigated.

In this paper, we present a methodology to estimate the ITF of a commercial SLS (the EinScan-Pro 3D Scanner) and its uncertainty. The ITF dependence on the tilt of the step artifact relative to the optical axis of the instrument was investigated and showed the importance of this alignment condition. The ITF dependence on the position in the measurement volume is also investigated. We found the ITF focusing distance is slightly different than the MTF. More interestingly, a comparison between ITF and Modulation transfer function (MTF) showed the ITF is slightly higher than the MTF at distances shorter than best focus. However, at the MTF's best focus (390 mm), the ITF agrees well with both MTF curves.

1.2 Theory

1.2.1 Definition of ITF

The ITF quantifies the instrument response to the spatial frequency content on the surface. The ITF is similar to the MTF of an imaging system, which describes how well the system images an object as a function of spatial frequency[10,11]. Similarly, ITF describes the instrument response to the spatial frequency on the surface to be measured. Like MTF, ITF is the ratio of the measured amplitude to the actual amplitude on the surface as a function of spatial frequency [10,11].

For a linear instrument response that is shift-invariant, the measurement can be modeled as the convolution of the height profile with the impulse response of the system:

$$g(x) = f(x) \otimes h(x). \tag{1.1}$$

Where *f(x)* is the input height profile, *h(x)* is the impulse response function, and *g(x)* is the measured height profile.

Taking the Fourier transform of Eq. (1), we get

$$G(f) = F(f).H(f), \tag{1.2}$$

where, *G(f)*, *F(f)* and *H(f)* are the Fourier transform of *g(x)*, *f(x)* and *h(x)*, respectively. The function *H(f)* is called the instrument transfer function (ITF), and is given by rearranging eq. (1.2),

$$H(f) = \left(\frac{G(f)}{F(f)} \right). \tag{1.3}$$

1.2.2 Method of Calculating ITF

Methodology to measure ITF depends on the choice of artifact and a discussion on the pros and cons of the artifacts is summarized in section 1.3.

Two methods can be used to calculate the ITF, the ratio method and the derivative method,

1.2.2.1 Ratio Method

This approach is a direct statement of the definition of ITF as described in section 1.2.1. In this approach, the ITF is taken to be the ratio of the Fourier transform of the measured amplitude to the Fourier transform of an actual amplitude. The advantage of using this approach is that any surface geometry can be used to measure instrument response. But this approach uses directly discrete Fourier transform of the surface geometry, which suffers from spectral leakage of the discrete Fourier transform. In addition to that this approach requires artifacts to be well-characterized.

1.2.2.2 Derivative Method (MTF standard Method)

The derivative method is the standard approach used for MTF measurements for digital imaging devices. It is well documented in ISO 1223 standards [12,13] and applies to only a step artifact for an ITF measurement or a knife-edge artifact in the case of the MTF measurement.

To calculate ITF by the derivative method, we calculate the derivative of the step edge response and then calculate the FFT of this line spread function. The validity of this approach is apparent by first considering a step profile function as

$$f(x) = step(x) \tag{1.4}$$

The output or measured step function is the input convolved with the impulse response function given by

$$g(x) = step(x) \otimes h(x) \tag{1.5}$$

The derivative of the measured step becomes

$$\frac{d}{dx}\big(g(x)\big) = \frac{d}{dx}\big[step(x) \otimes h(x)\big] = \left[\frac{d}{dx}\big(step(x)\big)\right] \otimes h(x) = \delta(x) \otimes h(x) \tag{1.6}$$

and taking the Fourier transform we see that

$$\frac{d}{dx}\big[step(x)\big] = H(f) = ITF \tag{1.7}$$

With this methodology we can avoid the spectral leakage issue but taking derivative dominates the noise.

1.3 Artifacts for ITF Measurement

Several artifacts can be used to measure ITF according to the literature. Each artifact has its pros and cons. The simplest artifact is a delta function, but it is practically impossible to construct a physical artifact like a delta function [14]. A sinusoidal surface can also be used, but it is difficult and expensive to make such an artifact. Also, using a sinusoidal artifact will give the ITF information only at one frequency, therefore many artifacts would be needed to approximately characterize the transfer function [14]. Alternatively, a chirped surface with a continuously-varying spacing could be used, in this case, the spatial frequency will vary continuously, but such surface usually has small amplitude (typically few microns for all spatial frequencies) [9] and is difficult to fabricate. Some researchers have proposed measurement of the ITF by measuring the corner of a cuboid as well [7,8]. A high-quality, very sharp, single step artifact is somewhat easy to fabricate and

intrinsically covers a wide range of spatial frequencies [14]. This is valid as long as the step is sufficiently sharp, that is the frequency content of the step is significantly higher than the instrument bandwidth.

The benefit of using a chirped surface is that they measure instrument response over the whole field of view, but there are several disadvantages as well. Artifacts like a chirped surface and the single sinusoid artifacts require that the artifacts be well-characterized. Also, from the above discussion, it is clear that these surfaces require the ratio approach for the ITF calculation, which suffers from spectral leakage due to the use of the discrete Fourier transform. Whereas the step provides an intrinsic DC signal which is well calibrated with the standard step height measurements, so the need to characterize becomes only a need to ensure that the step is sufficiently sharp. Measuring the corner of a cube is also a better choice over a chirped surface since a sharp corner of a cube covers a wide frequency range like a step artifact. The data can also be processed in a way to avoid spectral leakage [7]. However, the ITF calculation using a cube corner must still be based on the ratio method, therefore the height and angles must be well characterized in addition to the edge being sufficiently sharp.

1.4 Einscan-pro 3d scanner (A commercial structured light system)

In this paper, we describe a demonstration of the ITF measurement on a commercial structured light system-the EinScan-Pro 3D Scanner. The EinScan-Pro is a portable, lightweight, multifunctional 3D scanner that can be used in four different scanning modes: the handheld high density (HD) scan, the handheld rapid scan, the fixed scan with the turntable (Auto Scan), and the fixed scan without the turntable (Free Scan) [15,16]. The EinScan-Pro uses white LED-based projection scanning and delivers ‘watertight’ or ‘non-

watertight 3D data which can be used for 3D printing of real objects or can be used for reverse engineering applications [15,16] respectively. It uses two cameras and one projector to capture 3D point cloud data, and an optional external camera is available to enable full-color 3D [16]. Both cameras of the scanner were calibrated according to the scanner manual [15]. According to the manual, the suitable working distance is 350 to 450mm, the range and location over which a projected cross on the object can be seen. The manufacturer quotes a point spacing of 0.16mm for the fixed scan (auto and free) and 0.2~0.3mm for the handheld HD scan [15]. For our measurement, we used the fixed scan mode without activating the turntable.

Fig. 1-1. EinScan-Pro 3D Scanner.

1.5 Measurement object: step artifact

Based on the discussion in section 1.3, we decided to use the step as an artifact for ITF measurement. For an instrument like the EinScan-Pro with a resolution limit no better than the point spacing of 0.16 mm at best, a step artifact for an ITF measurement should have step edges with rounding on the scale of ~10 micrometers or better.

For the ITF to be a valid spatial resolution metric, the measurement must be within the linearity limits of the measurement. This means the step artifact should satisfy the following conditions [5,6]:

1. Geometric linearity condition: The surface height variation of the artifact should be much less than the distance between the camera and the projector.
2. Optical filtering linearity condition: the surface height amplitude should be smaller than the effective wavelength of the structured light measurement.
3. The artifact should contain a wide spatial frequency band.
4. The amplitudes of the sinusoidal components should be large compared to the typical measurement noise of the system.

No information about the effective wavelength and PSF of the EinScan was provided by the manufacturer. Visual inspection during a measurement of a flat plain white sheet provides an estimate of the effective wavelength and is about 2 mm for this system. The step artifact used for measurement was easy to make, contains a wide range of spatial frequencies, and had a step height of ~ 1 mm which meets the criteria of being much less than the working distance of the instrument (350-450 mm) and is less than the effective wavelength, satisfying both geometrical and optical filtering linearity conditions.

We created our step artifact by using a single crystal single-side polished Si wafer. Cleaving the wafer provided a nice straight and sharp edge. We epoxied two cleaved pieces of the wafer, polished sides down, to create a measurable step artifact. The unpolished side of the wafers, while relatively smooth, provided ideal light-scattering characteristics for the scanner. We measured the top and bottom terraces of the step with a scanning white light interferometer (SWLI) to characterize the artifact quality. The rms of each terrace (the unpolished side of the wafer) is about 0.6 μm. Assuming edge rounding on this same

scale, this artifact is well within the validity limits of the perfect step assumption as described above. Current edge measurements are underway to verify this assumption.

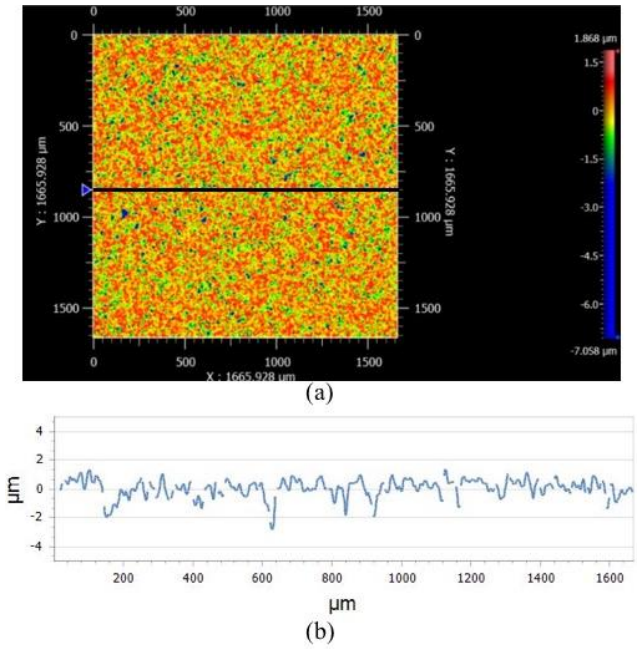

Fig. 1-2. SWLI measurement of top surfaces of the step artifact: (a) top surface, and (b) line profile along the line shown in (a).

For the measurements, the scanner was mounted on a heavy aluminum base and a precision rail and mount was used to quantify the position and orientation. The artifact was fixture to a prism table mount on the stage and a slight tilt angle could be varied. Measurement was taken at a different position in the measurement volume, which will be described in section 1.9. The working distance between the scanner and the artifact was measured to ±2mm. The experimental setup is shown in Fig. 1-3.

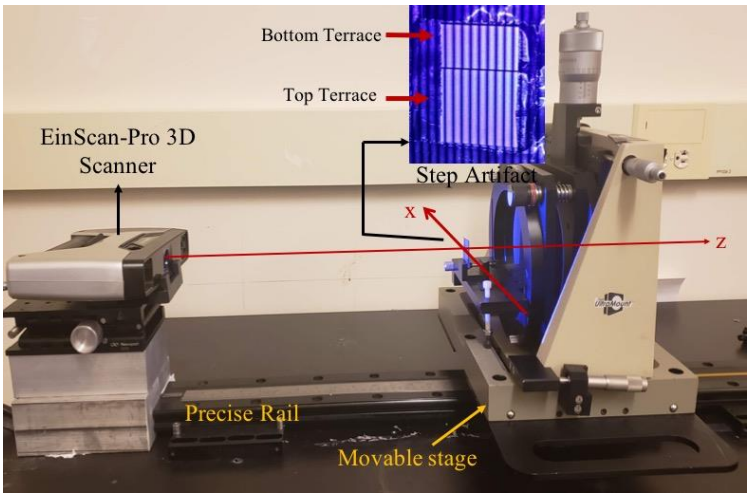

Fig. 1-3. Experimental Set-up for ITF Measurement.

1.6 Data processing for The ITF measurement

1.6.1 Coordinate Transformation

The point cloud data from the scan was imported into MATLAB, an example of which is shown in Fig. 1-4. This data is in the EinScan-Pro global coordinate system and needs to be transformed into a local coordinate system on the sample. This conversion is carried out in several steps and is summarized below:

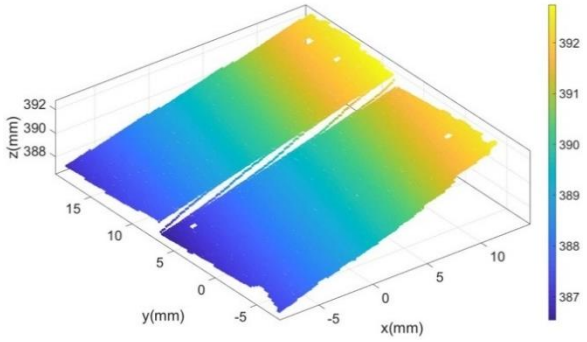

Fig. 1-4. Measured Point Cloud Data.

We first define the lower terrace as the reference plane by masking the lower level and fitting a plane. Conversion of data from the global to the local (see Fig. 1-5(a)) coordinate system to local coordinate system was done first rotation of the data about the z-axis and then the x-axis. For final rotation, we find the slope of the edge by picking two points close

to the edge and rotating the whole dataset about the z-axis such that the edge is parallel to the y-axis (Fig. 1-5 (b) and (c)). To find the correct alignment, we use a slope comparison approach [6], which uses the comparison of the slope of the step transition of the average step profile as a function of the angle used to align the edge of the step.

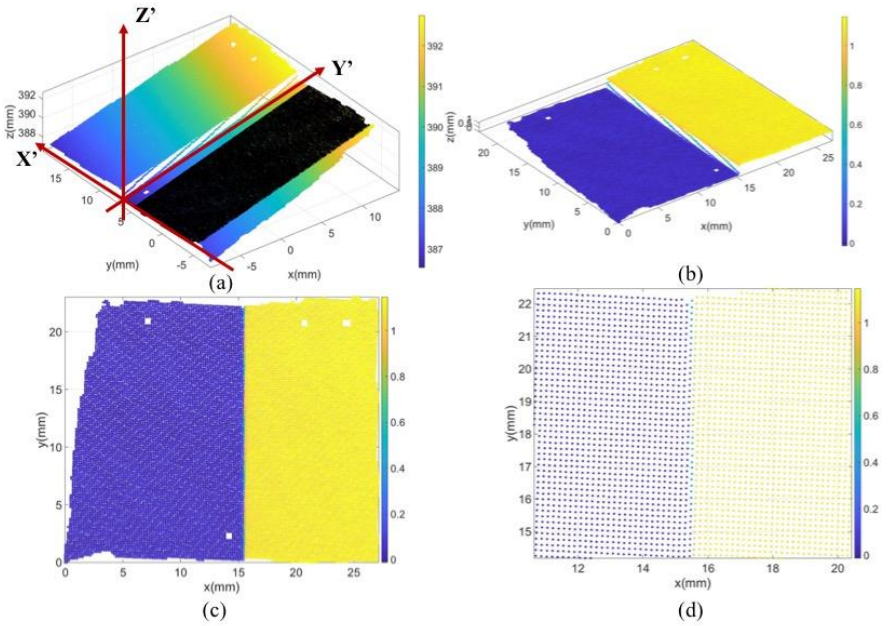

Fig. 1-5. (a) Define Local Coordinate System with a plane fit to lower terrace, (b) Data in Local Coordinate System, (c) Top View of Data in Local Coordinate System and (d) Presence of high frequency shoulder.

1.6.2 Average step profile to reduce measurement noise

Once we make the edge of the step profile parallel to the y-axis, all x-direction line traces are superimposed together to get a high-density 1-dimensional step profile, similar to the standard slanted edge method used for an MTF measurement. To reduce the measurement noise, we resample the 1-dimensional step profile and average the height values in each resampling interval to get an average step profile, as shown in Fig. 1-6(b).

The choice of the resampling interval is important [12,17, 18] should be fine enough to ensure that the ITF measurement is not re-sampling limited [12,17, 18]. The reported EinScan-Pro point spacing is at best Δx=0.16mm, corresponding to a Nyquist frequency of

3.12 cycles/mm. We oversampled our step profile by using a resampling interval of Δx/5, corresponding to a resampling frequency of 15.6 cycles/mm, which is well beyond the worst-case frequency limit of the instrument. Fig. 1-6(a) shows the resampled step profile with vertical lines showing the resampling intervals.

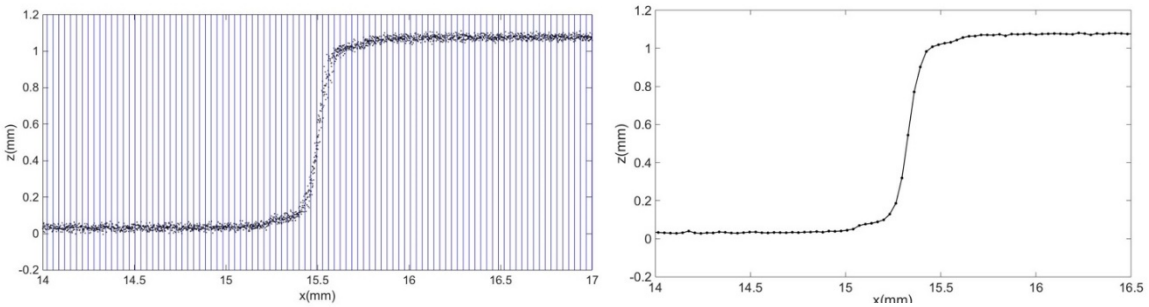

(a) (b)

Fig. 1-6. (a) Resampling of higher density 1-D step profile, and (b) Average step profile.

A high-frequency shoulder is observable in the average step profile (see Fig. 1-6(b) and 1-5(d)) that is not expected in a simple impulse response convolution model. The structure is an artifact of the line profile averaging process and the discrete sampling interval in the point cloud data. Since the step was at a slight angle to the global y-axis of the instrument, Moiré beating between the point cloud sampling period and the step angle causes finer structure in the average step profile. This effect is discussed in the context of MTF measurements for a sampling-limited system and is best handled by filtering and/or averaging [17,18].

We took a filtering approach in this analysis, and filter out this noise by modeling the convoluted step measurement with a Sigmoid function. This analytic function is a good approximation to the convolution of an impulse response with a step function [19] to it, which will be the best estimate of the average step profile of step measurement. The fitting

removes the shoulder artifact and reduces the noise. The Sigmoid fit to the average step profile is shown in Fig. 1-7.

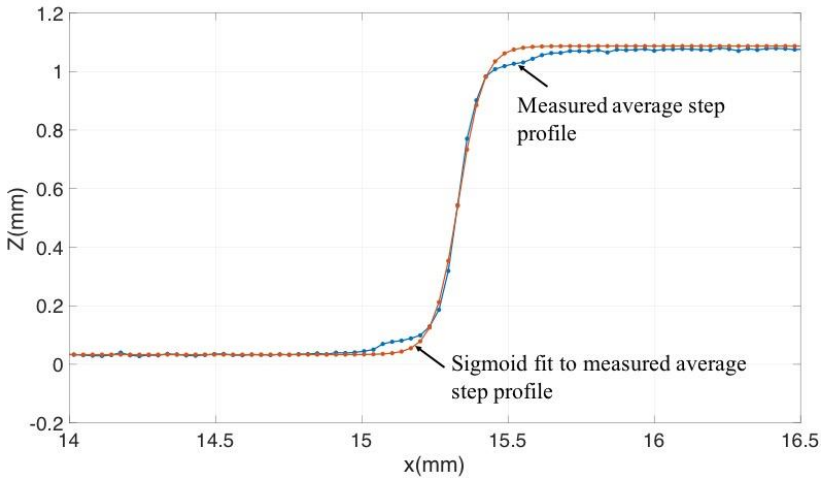

Fig. 1-7. Sigmoid Function fit to the measured step profile.

1.6.3 Calculation of ITF

Using the derivative approach discussed in section 1.2.2.2, we calculate the derivative of the Sigmoid function fit to the average step profile and use this to calculate the line spread function (LSF). Finally, the ITF calculates as the Fourier transform of the LSF. the LSF and ITF curves are shown in Fig. 8(a) and 8(b), respectively.

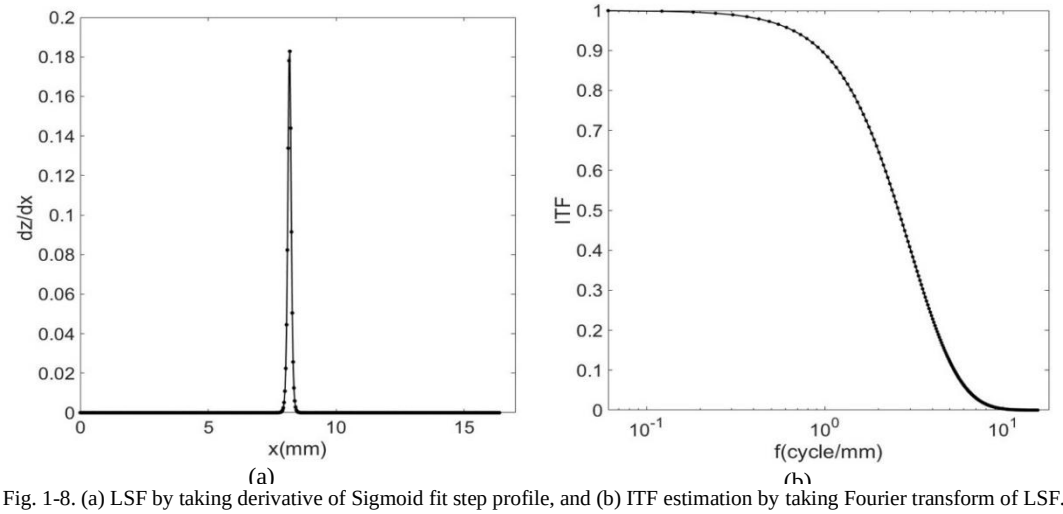

Fig. 1-8. (a) LSF by taking derivative of Sigmoid fit step profile, and (b) ITF estimation by taking Fourier transform of LSF.

1.7 Uncertainty Analysis for The ITF measurement

Several quantities affect the ITF measurement including environmental factors (such as humidity, temperature, and vibrations, etc.), process parameters (such as estimation of angle for alignment), and instrument noise. Environmental factors and instrument noise can be evaluated with a repeatability test. We repeat the ITF measurement ten times and take the average of the ten measurements as the best estimate of the ITF. The repeatability uncertainty, then, is the standard deviation of the mean (the standard deviation of the ten results divided by $\sqrt{10}$ [20]).

Process parameter choices also affect the ITF calculation and, in this case, dominate the combined uncertainty. The angle estimation for aligning the step edge is the largest contributor. The best estimate of the optimum angle is 12.9° ± 0.2° and the uncertainty due to this is estimated by repeating the ITF calculation using 12.7° and 13.1°, respectively, and then taking the average of this change. The combined uncertainty for ITF at each frequency point is then estimated by combining the standard uncertainty due to repeatability with the Total uncertainty was estimated by calculated standard uncertainty for angle estimation in a root-sum-square fashion.

The best estimate of ITF along with uncertainty (coverage factor=2) at a working distance of 380 mm is shown in Fig. 1-9. The spatial frequency at which ITF falls to 50%, the cutoff frequency, is 2.6 ±0.5 mm^{-1}. The corresponding cutoff wavelength is around 0.38 mm.

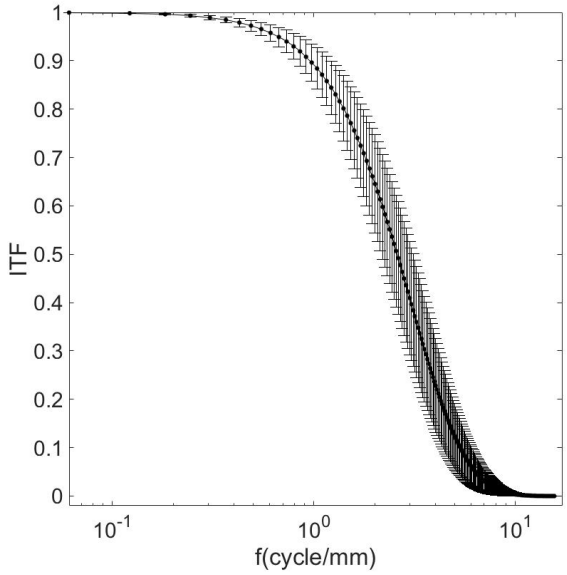

Fig. 1-9. The best estimate of ITF along with uncertainty at 380mm.

1.8 ITF as a function of step orientation

The tilt of the step with respect to the scanner is an important consideration. A tilt in one direction will lead to shadowing (taken to be a negative tilt angle) and too much tilt in the other direction will violate the assumptions of the model. The impulse response is defined along the measurement axis and the measurement is modeled as a convolution of this impulse response with a step profile. This model will not match the measurement if the step is tilted too far from the measurement axis. We explored these limits by repeating the ITF measurement for a range of step tilt angles varying from -25^{o} to 20^{o} in 5^{o} increments.

For negative tilt angles, shadowing is observed as data drop out. This can be seen by plotting the number of points in each resampling interval (Fig. 1-10 (a)) and it is observed as a gap in data at an apparent step edge when the negative tilt angle becomes significant (see inset). At positive tilt angles beyond 10 ^{o} the line profile data begins to show an undercut characteristic (Fig. 1-10 (b)) which we interpret to mean that the model assumptions are breaking down. The trend can be seen by plotting the slope of the step

transition as a function of tilt angle (see Fig. 1-10(b)). The slope increases as the tilt angle increases up to $10^{o.}$ Beyond 10^{o} the slope is negative (see inset for 20^{o} in Fig. 1-10(b)), suggesting that the model assumption is not valid at higher positive angles. Measurements and simulations are underway to investigate this in more detail. For the data discussed here, a positive tilt angle of ~ 2^{o} was used for all measurements that follow.

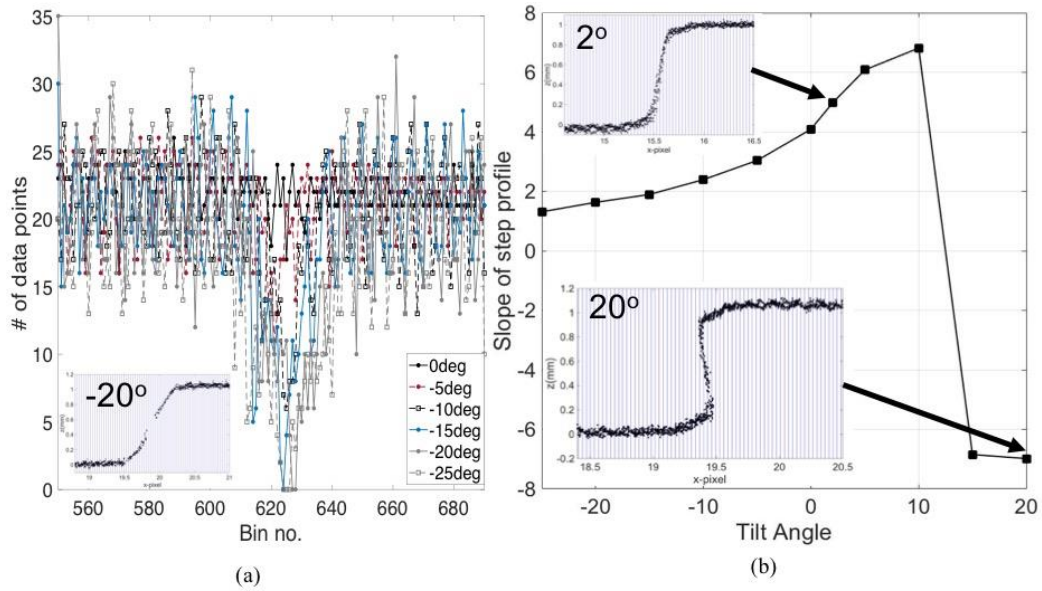

Fig. 1-10. ITF dependence on step orientation. (a) No. of data points as a function of bin no. for negative angles and (b) Slope of the step transition as a function of angle for all tilt angles.

1.9 ITF as a function of WORKING distance

The ITF dependence on the position along the measurement axis was also investigated. The working distance was varied from 350 to 450 mm in steps of 10mm, covering the manufacturer's recommended working distance range. The ITF is approximately the same from 350 mm to 410 mm, with the best ITF occurring at 380 mm, which we refer to as the best focus. The behavior over the full range can be appreciated from a plot of the 50% cutoff frequency as a function of distance (Fig. 1-11), emphasizing the best focus behavior for 380 mm. The ITF is approximately symmetric for an equal amount of defocus.

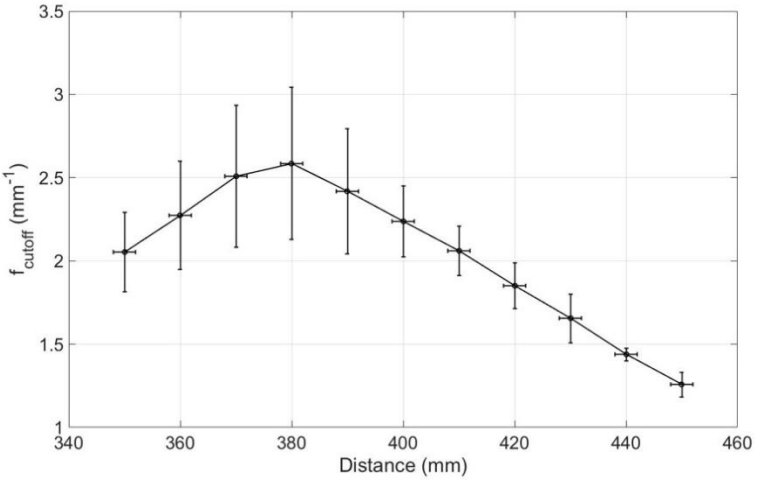

Fig. 1-11. The ITF cutoff frequency as a function of distance.

1.10 MTF Vs ITF

Many optical-based measurements use a camera for data acquisition and this will necessarily impose a limit on the instrument resolution. Based on literature for interferometery[3,4] and deflectometry[10], the ITF is expected to agree with the MTF of the camera within the linearity limits of the measurement. The theory has been discussed for a fringe projection system, predicting that the ITF and the MTF should be the same as long as 1) the surface variation is much smaller than the effective wavelength and 2) the width of the PSF is much smaller than the effective wavelength[6]. The instrument used here has two cameras, and the MTF of each camera was measured and compared to the ITF to evaluate this prediction.

The standard slanted edge MTF testing method was followed (ISO 12233[12-13]). For each measurement, the projector of the scanner was blocked and pictures were taken with each camera of the back-illuminated razor blade. The edge of the razor blade was slightly tilted relative to the camera detector array axes to apply the slanted edge approach. An example of an image used for the MTF measurement is shown in Fig. 1-12. The processing steps for the MTF measurement can be found in the literature [12-13].

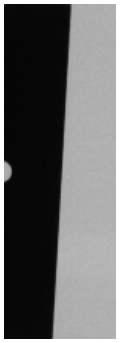

Fig. 1-12. An image of the slanted knife edge for the MTF measurement.

The MTF was also measured at different positions in the measurement volume at similar distances as used for ITF measurements. The best focus MTF of both cameras is at approximately 390 mm, which is about 10 mm shifted from the position where the best ITF was measured. However, similar to ITF, the MTF is also almost the same from 370 to 400 mm. The comparison of the MTF of both cameras shows that the MTF of camera-2 is slightly better than the MTF of camera-1 from 380-450mm and that the MTFs of both cameras are approximately the same from 350-380 mm. Similar to the ITF, the MTF is also approximately symmetric about its best focus.

A comparison between ITF and the MTF of both cameras shows that the ITF is slightly higher than the MTF at distances shorter than the best focus. This may be a consequence of the phase-shifting algorithm's insensitivity to fringe contrast and the MTF's direct attenuation of irradiance contrast[5]. However, at the MTF's best focus (390 mm), the ITF agrees well with both MTF curves. A comparison of the ITF and the MTF for each camera at 350 mm, 390mm, and 450mm is shown in Fig. 1-13.

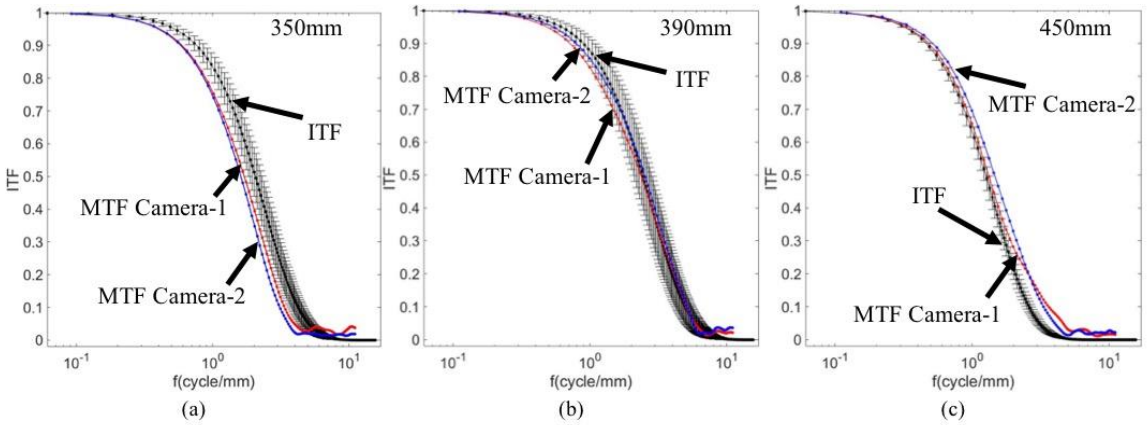

Fig. 1-13. Comparison of ITF and MTF of Camera-1 and Camera-2. (a) At 350mm, (b) at 390mm (MTF best Focus), and (c) At 450mm.

To summarize this result, the cutoff frequencies for ITF and the two MTF curves were plotted against, including uncertainty estimates in both distance and cutoff value (Fig. 1-14). The plot shows that ITF shows better frequency response than either MTF at positions closer than 380 mm, and the ITF falls close to the MTF of camera-1 at distances beyond the best focus.

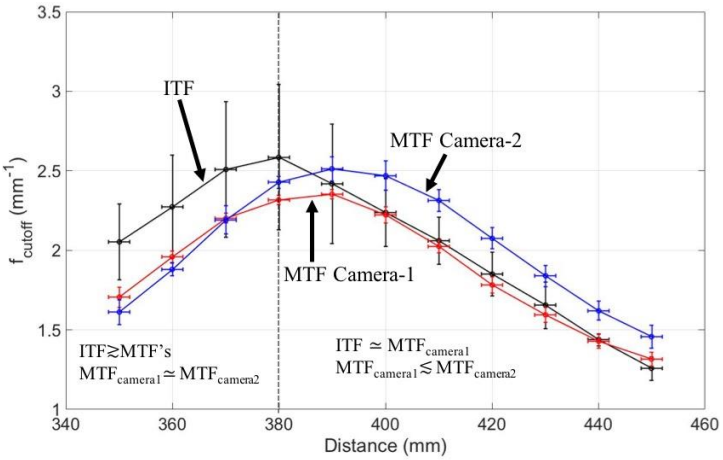

Fig. 1-14. Comparison of ITF and MTF's as a function of distance.

1.11 Conclusion

A methodology to measure the ITF of a commercial structured light system (the EinScan-Pro 3D Scanner) and its uncertainty has been developed. The ITF dependence on

the tilt of the step artifact relative to the optical axis of the instrument was investigated and showed the importance of this alignment condition. The investigation of ITF as a function of working distance shows that the best frequency response is found at 380 ± 30 mm and that the ITF reduces systematically about the best focus condition. The MTF of each camera was also examined as a function of working distance. The best focus conditions for camera-1 and camera-2 are 390 ± 10 mm. A comparison of ITF with MTF shows that the ITF is slightly higher than the MTF at positions closer than best focus and the ITF is close to the lower MTF of camera-1 for distances beyond the best focus.

As mentioned above discussions, in the literature suggest that the ITF follows the MTF and that the MTF can be used as the measure of spatial resolution. The theoretical analysis by Zhang, et al. showed the equivalency of MTF and ITF in the limit that the PSF is small compared to the effective wavelength[6] and this is the case over the defocus range investigated here. A more rigorous comparison of ITF and MTF would require lower uncertainty ITF measurements. Also, the use of MTF to estimate the spatial frequency response for an instrument like the EinScan that has two cameras, the MTF of both cameras should be measured and compared. For applications that require a strong statement of spatial resolution with low uncertainty the question of a direct ITF measurement versus an MTF measurement of the cameras should be considered carefully.

ACKNOWLEDGEMENTS

This work would not have been possible without the financial support of the Center of Precision Metrology. We thank Scott Williams, Jeffery Thousand, and Michael Dhooghe for their assistance in the experimental setup and Mr. Greg Caskey for his help with scanning white light interferometer (SWLI) measurements.

REFERENCES

1. der Jeught, S. V., and Joris, J. J. D., “Real-time structured light profilometry: a review,” Optics and Laser Engineering 87, 18-31(2016).
2. Gupta, M., Agrawal, A., Veeraraghavan, A. and Narasimhan S.G., “Structured light 3D scanning in presence of global illumination,” Proc. CVPR, 713-720, (2011).
3. Xavier, C. d. L. and de Groot. P. J.,” Lateral resolution and instrument transfer function as criteria for selecting surface metrology instruments,” Imaging and Applied Optics Technical Digest, OTu1D4, (2012).
4. de Groot, P., Lega, X. C. De., de Lega, X. C., “Interpreting interferometric height measurements using the instrument transfer function,” Fringe 2005, 30–37, Springer Berlin Heidelberg, Berlin, Heidelberg (2006).
5. Zhang, B., D. Allen, A., Ziegert, J., and Evans, C., “Validity of the instrument transfer function for fringe projection metrology,” Applied Optics, Vol 57, No. 11, 2795-2803 (2018)
6. Zhang, B., D. Allen, A., Ziegert, J. and Evans, C., “Application of instrument transfer function to a fringe projection system for measuring rough surfaces,” Proc. SPIE 10373, 103730S (2017).
7. Berssenbrügge, P., Dekiff, M., Kemper, B., Denz, C.., Dirksen, D., “Characterization of the 3D resolution of topometric sensors based on fringe and speckle pattern projection by a 3D transfer function,” Opt. Lasers Eng. **50**(3), 465–472 (2012).
8. Kellner, T., Breitbarth, A., Zhang, C. and Notni, G., “Characterizing 3D sensors using the 3D modulation transfer function,” Measurement Science and Technology, 29,1-8 (2018).

9. Leach, R., Giusca, C., Henning, A., Sherlock, B. and Coupland, J., “ISO definition of resolution for surface topography measuring instruments,”, Fringe, 405-410 (2013).

10. Tianquan, S., Maldonado, A., Su, P., Zhou, P. and Burge, J.H., “Study of the instrument transfer function of a free-form optics metrology system: SCOTS,” Proc. SPIE 9046,904602, 904602-1-904602-7 (2013).

11. Tianquan, S., Maldonado, A., Su, P., Zhou, P. and Burge, J.H.,” Instrument transfer function of slope measuring deflectometry systems,” Applled Optics, 2981-2990 (2015).

12. Eichenbach, S.E., Park, S.K. and Naranswamy, R., “Characterizing digital acquisition devices,” Optical Engineering 30, 170-177 (1991).

13. Masaoka, K., Yamashita, T., Nishida, Y. and Sugawara, M., “Modified slanted-edge method and multidirectional modulation transfer function estimation,” Optics Express 22, 6040-6046 (2014).

14. Takacs, P. Z., Li, M. X., K. Furenlid, and Church, E. L., “A step-height standard for surface profiler calibration,” Optical Scattering, 235–244 (1993).

15. EinScan-Pro user manual

16. <https://www.einscan.com/handheld-scanner/einscan-pro/> (14 July 2019).

17. Boreman, G. D., [Modulation Transfer Function in Optical and Electro-Optical Systems], SPIE Press, Bellingham, Washington (2001).

18. Park, S.K., Schowengerdt, R. and Kaczynski, M.A., “Modulation-transfer-function analysis for sampled image systems,” Applied Optics 23, 2572-2582 (1984).

19. Iliev, A., Kyurkchiev, N. and Markov, S., “On the approximation of the step function by some sigmoid functions,” Mathematics and Computers in Simulation 133, 223-234 (2017)

20. Bevington, P.R., Robinson, D.K., [Data Reduction and Error Analysis for The Physical Science], Mc Graw Hill, (2003).

Chapter 2. ESTIMATING UNCERTAINTY FOR THE INSTRUMENT TRANSFER FUNCTION MEASUREMENT OF 3D SCANNERS

ABSTRACT

Spatial resolution is an important aspect of many optical instruments. It is defined as the ability to faithfully output the fine detail present in the input. Following convention, spatial resolution can be defined as the spatial frequency response of the instrument, known as the instrument transfer function (ITF). In this paper, we describe the step-artifact approach for estimating the ITF for 3D scanners, discuss step artifact characterization and validation approaches, and present a method to estimate the combined uncertainty of the ITF measurement. The approach is demonstrated using the EinScan Pro 3D scanner. A step artifact is used for the measurement that takes advantage of the cleaving properties of a single-side polished silicon wafer. The uncertainty analysis includes simulations to estimate the contribution due to influencing factors such as the alignment of the step artifact to the measurement axis, the diffuse vs. specular scattering properties of the step edge, and various processing parameter choices.

2.1 Introduction

In recent years, structured light systems (SLS) have become popular for acquiring 3D geometric measurements because they are non-contact and fast. The applications are diverse, benefitting sectors such as medical, industrial automation, and entertainment technology [4,5]. The measurement is based on the principle of triangulation and a variety of commercial instruments are available. The quantitative measurement result is increasingly relied upon and the spatial resolution, or fidelity with which fine features on the surface are captured, is an important aspect to understand. The point spacing specification of the instrument is often an optimistic prediction of the resolution. A

measure of the spatial frequency response, known as the instrument transfer function (ITF), is the preferred metric [1-3]. The instrument transfer function is analogous to the modulation transfer function (MTF) of imaging systems, like the cameras used in 3D scanning devices [1-3,6-9]. The MTF captures the image contrast resolution whereas the ITF captures the height profile resolution. There is an ISO standard (ISO 25178-604) that defines the resolution limit for 3-dimensional measurements as the spatial frequency at which the ITF falls to 50%, known as the lateral period [1,12]. The study of ITF for 3D scanners is limited and only a few publications are available [3,10,11]. A complete discussion on estimating the combined uncertainty for an ITF measurement has not been discussed.

In this paper, we present a methodology to estimate the ITF of a commercial SLS (the EinScan-Pro 3D Scanner) following the step-artifact approach with a complete uncertainty analysis. We introduce the use of a step artifact that is fabricated from a single-side polished silicon wafer and include a discussion of characterizing and validating the step artifact. The single crystal cleaving property of the wafer yields a very sharp step edge artifact, but the face of the step is specular rather than diffuse (the ideal surface characteristic for good 3D scanner measurements). The consequence of a specular vs diffuse step face is considered in the comprehensive combined uncertainty analysis in addition to influence factors such as the focus condition, position in the measurement volume, step alignment, and various data analysis processing parameters.

2.2 Theory

The ITF is closely related to the MTF of an imaging system, with the ITF defining the spatial frequency response of the height information in the output rather than the spatial

frequency response of the irradiance profile in the image plane for MTF. Mathematically, the ITF is defined as the ratio of the measured height amplitude to the actual height amplitude as a function of spatial frequency [3,6,7,13].

For a linear and shift-invariant system, the output *g(x)* can be defined as the convolution of the input *f(x)* and the impulse response function *h(x)*:

$$g(x) = f(x) \otimes h(x) \tag{2.1}$$

Taking the Fourier transform of Eq. (1), we get

$$G(f) = F(f).H(f) \tag{2.2}$$

where, *G(f)*, *F(f)* and *H(f)* are the Fourier transform of *g(x)*, *f(x)* and *h(x)*, respectively. The function *H(f)* is called the instrument transfer function (ITF) and is given by rearranging Eq. (2),

$$H(f) = \frac{G(f)}{F(f)} \tag{2.3}$$

Linearity of the measurement – a proportionality relationship between input and output - is an essential condition for the use of a frequency-response-based resolution description like the instrument transfer function. A consequence of linearity is that the frequency content simply adds without frequency mixing, i.e., if two frequency components are present in an input signal, the output is the simple sum of the response to each frequency component [7]. If a system is not linear, the output signal will contain spatial frequencies other than those of the input signal [5]. Structured light systems are approximately linear systems when the following two conditions are fulfilled [13,14]:

1. The amplitude of each sinusoidal component on the surface satisfies the geometric linear constraint, that is the surface height variation is much less than the working distance (distance between the camera and the object) [13,14].

2. The width of the point spread function (PSF) is small compared to the carrier wavelength of the system [13,14].

We will discuss approaches to checking that the ITF characterization has been carried out in the linear limit of the instrument in a future publication.

The ITF can be calculated in two ways [3,13], 1) the ratio method which uses artifacts with engineered and well-characterized frequency content (examples are given in references 7, 10, 12, 17, 18, 19, and 20) and 2) the derivative method which uses a step artifact [3,13]. Any type of artifact can be used for the ratio method provided it contains the frequency content of interest for the characterization, but it must be dimensionally well characterized and can be difficult to both fabricate and measure [3,22]. Also, the division operation with the ratio method leads to noise amplification in the high frequency limit [3]. With the derivative approach using a step artifact, the ITF is the normalized Fourier transform of the derivative of the step profile [3], and as such does not require a rigorous dimensional characterization, provided the step edge is sufficiently sharp [3]. Sufficiently sharp means that the frequency roll-off at high frequencies of the actual step must occur at frequencies well beyond the frequency cutoff of the instrument to be characterized, as shown in Fig. 1. The detail of checking the validity of the step artifact is discussed in section 2.4.1.1. The derivative method with the use of a step artifact is used for the analysis discussed here.

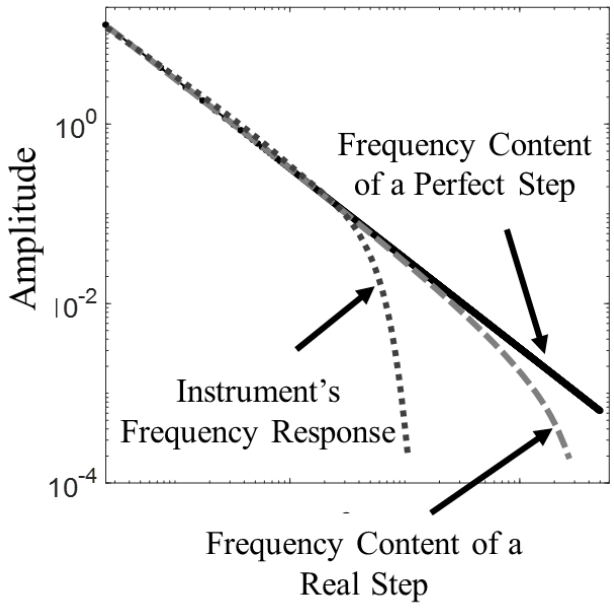

Fig. 2-1. Validity limit of a step artifact.

For the uncertainty analysis, we start with a clear definition of the measurand – the goal is to estimate the instrument transfer function along the measurement axis at best focus within the measuring volume (X±10 mm Y±10 mm Z±5 mm) (see Fig. 2-3) under a specified environmental condition. The measuring volume is selected based on the size of the artifact used and a sensitivity investigation confirming that the ITF does not appreciably vary over the size of the artifact. We carry out the ITF measurement and demonstrate the uncertainty analysis for an EinScan-Pro 3D-scanner. The EinScan-Pro uses white LED-based projection scanning and is a portable, lightweight, multifunctional 3D scanner that can be used in four different scanning modes: the handheld high density (HD) scan, the handheld rapid scan, the fixed scan with the turntable (Auto Scan), and the fixed scan without the turntable (Free Scan) [15,16]. We used the fixed scan mode without activating the turntable for the measurements discussed here. The EinScan-Pro uses two cameras and one projector to capture the 3D point cloud data. The scanner is calibrated according to the

scanner's user manual [15]. The manufacturer quotes the working distance as 350 to 450mm with a point spacing of 0.16 mm for the fixed free scan mode [15].

We fabricated a step artifact for the measurement from cleaved pieces of a single-side polished silicon wafer. The unpolished wafer surface is oriented up and the surface roughness causes sufficient diffuse scattering for good fringe visibility without having to overcoat the sample (see Fig. 2-2(a)). The cleaving process results in a very sharp edge, and the cleaved edge is used for the step by affixing a top cleaved piece upside down to a second upside down piece (see Fig. 2(a)). A cross-sectional schematic of the step artifact is shown in Fig. 2-2(b). Care is taken to minimize the gap between the pieces and ensure that the bottom edge of the step is not compromised with excess adhesive. The wafer is 1 mm thick, resulting in a step height of ~1 mm, which satisfies the linearity requirements explained above for the system.

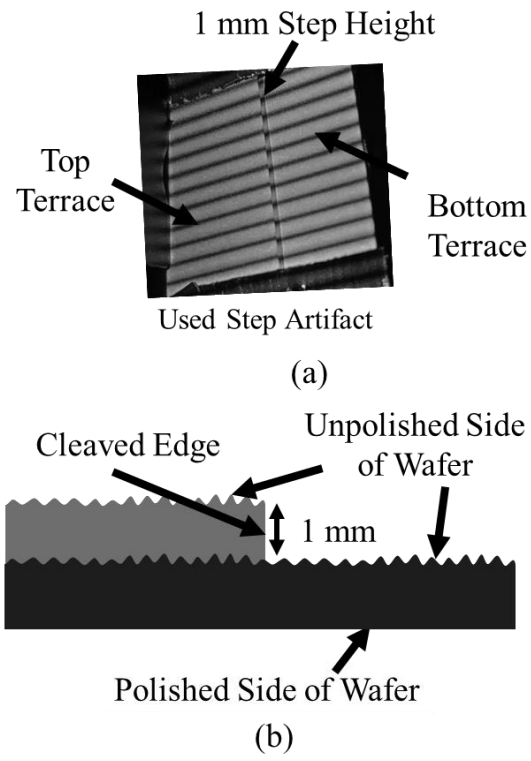

Fig. 2-2. (a) Photograph of the step artifact used for the ITF measurements and (b) cross-section schematic of the sample.

2.3 Data Processing

The details of the data processing for the ITF measurement are described in reference 3. The main steps are i) calculate the average line profile of the step in a local coordinate system from the measured point cloud data, ii) fit a Sigmoid function to minimize the impact of high frequency noise, iii) take the derivative to estimate the line spread function (LSF), and iv) take the Fourier transform to estimate the ITF. The data processing steps must each be considered in the uncertainty analysis. The main steps to consider are

The coordinate transformation (masking the lower terrace, plane fit to masked region, and defining a local coordinate system).

calculation of the average step profile (angle estimation to rotate the step parallel to the y-axis and the choice of the resampling interval).

impact of noise on the Sigmoid fit to the measured step data. (Repeatability)

The experimental setup is shown in Fig. 2-3.

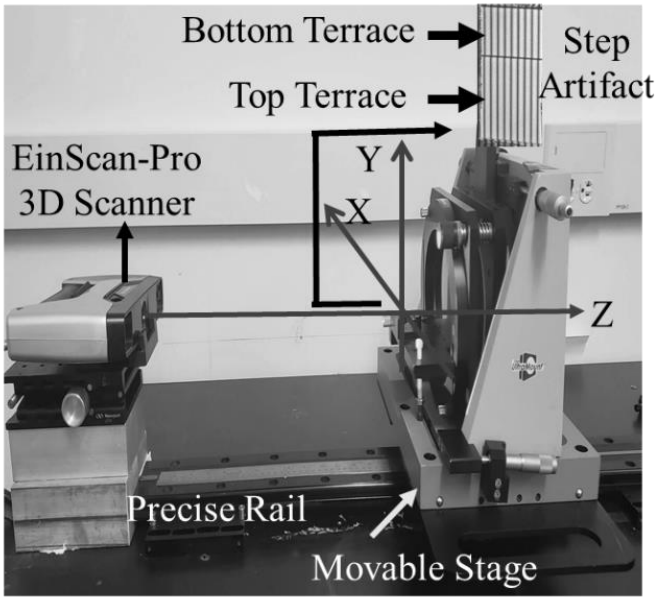

Fig. 2-3. Experimental set-up for ITF measurement.

2.4 Uncertainty Analysis

Several quantities can affect the output probability distribution function (PDF) of our measurand including environmental factors, experimental procedure, and each step of data processing. We divided these contributors into five categories: model assumption (includes step artifact assessment), measurement (experimental procedure), environmental factors, coordinate transformation, and the calculation of average profile. The influence quantities in each category are summarized in the fishbone (Ishikawa) diagram shown in Fig. 2-4. Consideration of each is discussed below and the standard uncertainty estimated for those found to be significant. Many of these contributors are negligible if care is taken in fabricating, positioning, and aligning the artifact as discussed below.

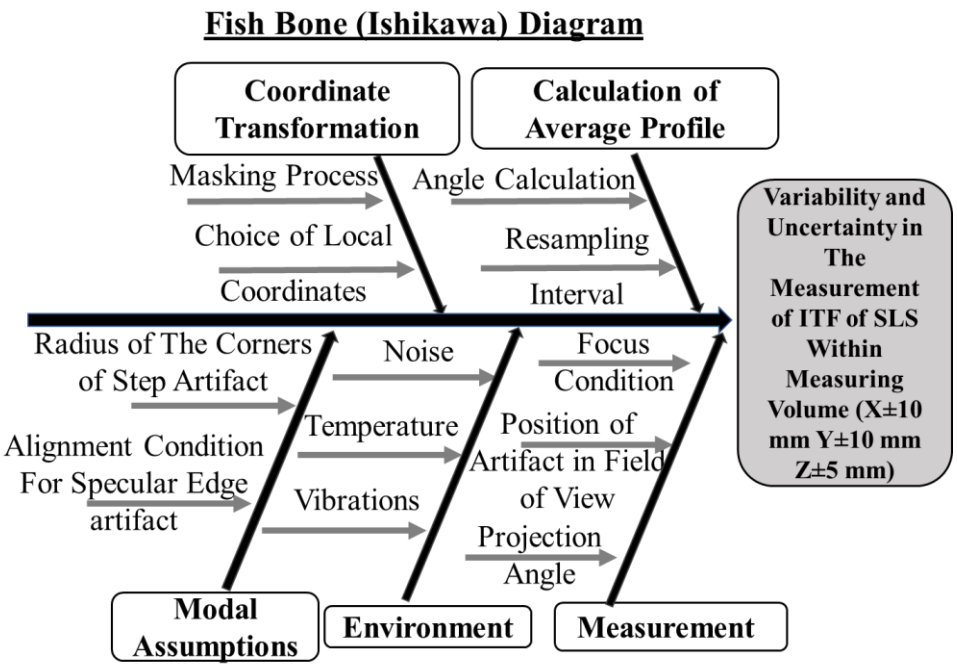

Fig. 2-4. The fishbone diagram

2.4.1 Model Assumption

The calculation of the ITF from a measurement of a step is based on the assumption that the step artifact is perfect – which is never the case. A perfect step has infinite frequency content (see a black curve in Fig. 2-1) and a real step is not perfectly sharp which means the rounded edge leads to a drop off of frequency content (see blue curve in Fig. 2-1). Another assumption is that the measurement responds equally to the surfaces of the step, meaning uniform scattering properties of the artifact.

2.4.1.1 Radius of the corners of step artifact

A real step artifact does not contain infinite spatial frequency content and therefore rigorously violates the model assumption, but it can be used to approximate a perfect step for the measurement as long as the frequency content drop off is far beyond the frequency response (ITF) of the instrument (see Fig. 2-1). The frequency at which the amplitude begins to drop below the expectation for a perfect step is related to the radius of curvature

of the step. We measured the radius of the top corner of the step artifact and used this with simulation to estimate the frequency content of the artifact. We used a scanning white light interferometer to measure the step edge, and the measurement is challenging due to the different scattering properties of the step edge and the surface and the numerical aperture constraint of the objective on the scanning white light interferometer. Hence the step edge is measured (Fig. 2-5(a)) by placing a similar cleaved wafer at a small ~5^{o} angle, cleaved face up. We estimate the radius by masking the corner and carrying out circular least-squares fits. We estimate the radius to be 1.8 ± 0.5 μm (Fig. 2-5(c)). The lower corner is difficult to measure and we reasonably assume it is likely to undercut slightly as shown in Fig. 2-5 (b). We can assess the potential impact of this finite-curvature step edge in a few ways. First, we generate a 1-mm high step profile with a rounded ~2μm radius corner. We then process this profile as through it were a measurement output, thereby generating an ITF curve that would be the apparent frequency response (ITF) if the measurement were limited by the step artifact geometry. This is the dotted gray curve shown in Fig. 2-6 (a). For a visual of the sensitivity to the corner radius, we repeated this process using a 1 mm height step profile with a 5X-larger corner radius (10-μm corner radius). This is the black curve in Fig. 2-6 (a).

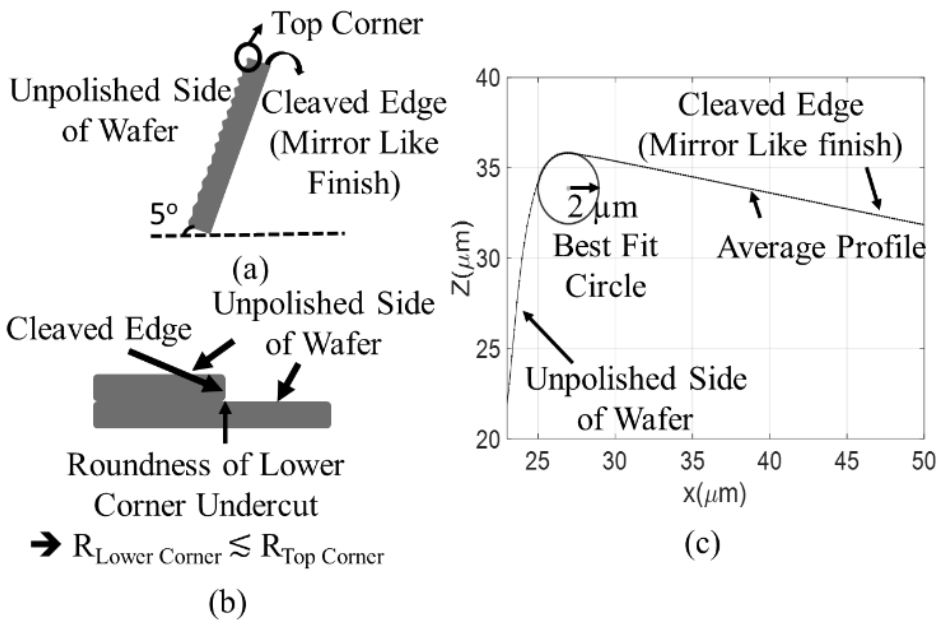

Fig. 2-5. (a) Measurement condition for the top corner of the step artifact, (b) The roundness of the bottom corner is undercut. and (c) Measured radius of the top corner.

Now we assess these curves compared to a best-case prediction of the frequency response of the instrument – which is a frequency response limited by the point spacing of the measurement. We estimate this limiting frequency response (ITF) by generating a Gaussian line spread function (LSF) with a 0.16 mm width, the Fourier transform of which we take to be the best-case response of the system. This is the gray curve in Fig. 2-6(a). The comparison of the three curves in Fig. 2-6(a) shows that a step artifact even with a corner radius of 10 μm (higher than the measured corner radius (2 μm)) can be used for the ITF measurement.

We can also evaluate the quality of the step artifact in the spatial domain by generating a step profile with the 10 μm radius corner and comparing it to a simulated measurement of a perfect step with the instrument when it is given the best-case impulse response for the instrument using the 0.16 mm FWHM Gaussian LSF. The comparison of the step artifact profile with a 10-μm radius corner and the convolution of this best-case LSF with a perfect

step (gray profile) is shown in Fig. 2-6(b). This spatial domain comparison is also a good visual confirmation that our step is sufficiently sharp to be considered a perfect step for the ITF measurement. This simulation exercise suggested a rule of thumb that the radius of the step artifact should be less than roughly half of the point spacing of the scanner. In this limit, the finite curvature of the step edge will not significantly contribute to the ITF measurement uncertainty.

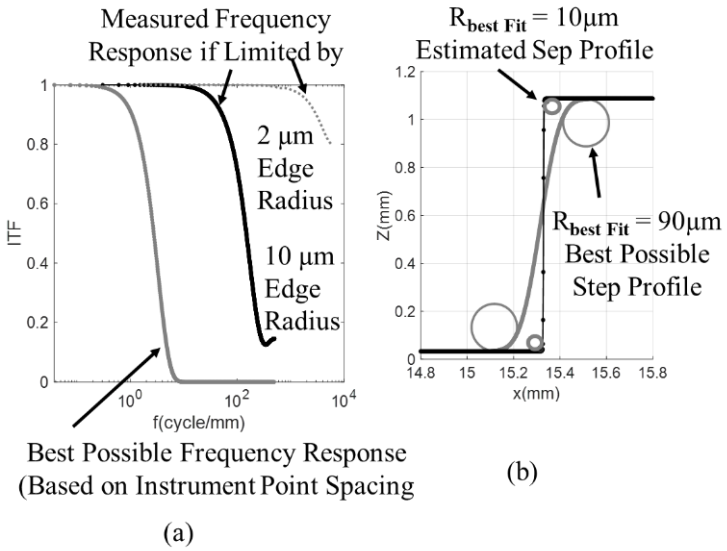

Fig. 2-6. (a) The frequency response of the estimated step profile by measured radius and with 10 µm corner radius step profile is far beyond the best possible frequency response when limited by instrument LSF. (b) Two steps created using. (1) the artifact step radius (10 µm) and (2) the best possible step profile when a line-spacing-generated LSF is used.

2.4.1.2 Alignment condition for a specular edge artifact

Alignment is another important aspect of the ITF measurement. The model assumes that the face of the step is aligned with the measurement axis. This will never exactly be the case, so the impact of alignment uncertainty on the final ITF uncertainty must be considered. Consideration of this uncertainty is especially important with our silicon-cleaved artifact because the end face of the step is specular and is not directly detected by the instrument. We investigated this effect experimentally and with simulation.

Experimentally we repeat the ITF measurement for a range of step tilt angles varying from -20° to +20° in 5° increments and at +2° as shown in Fig. 2-7.

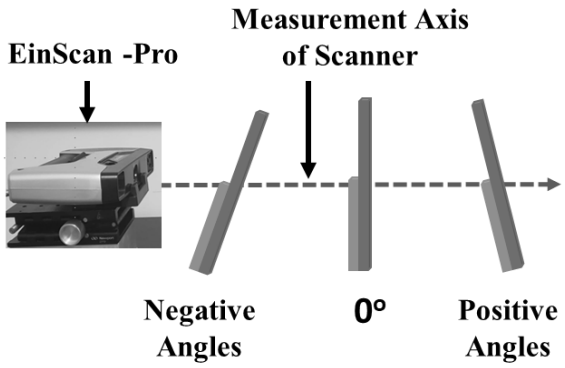

Fig. 2-7. Tilt condition of the step artifact about the measurement axis.

Tilt in the negative direction leads to shadowing and appears as a clear gap in the data at the step profile (see a middle figure in Fig. 2-8(a)). Presumably, this is because the instrument uses two cameras at slight angles to the measurement axis. For this reason, a slightly positive angle is best to avoid shadowing. This gap can be quantified by plotting the number of points in each resampling interval (bottom figure in Fig. 2-8(a)). Tilt in the positive direction leads to an undercut step profile (a negative slope at the step after the coordinate transformation data processing step (Fig. 2-8(b)). This is because of the imaging properties of the specular edge. The specular face of the step optically behaves like a mirror so the instrument will image and consequently measure the specular reflection of the bottom terrace diffuse surface as shown in Fig. 2-9(a). This effect is observed with simulation, as well. For the simulation, we start with a perfect step and rotate the step to different angles along the measurement axis in 5° increments from 0° until +25° and also at +2°. At each angle, the law of reflection is applied to the specular part of the profile as shown with the dotted gray line in Fig. 2-9(a). The reflection-modified profile at each angle is then convolved with 0.16 mm FWHM Gaussian. The simulated data is then rotated

back to a horizontal alignment, as would be done with the experimental data, resulting in a clear undercut step profile. This shows that a specular edge artifact can be used, but the step must be carefully aligned to the measurement axis. From the simulation, we can estimate an alignment goal and uncertainty for a limit in which misalignment will not significantly contribute to the ITF measurement uncertainty. We find this to be $+1^{o} \pm 1^{o}$ for our system.

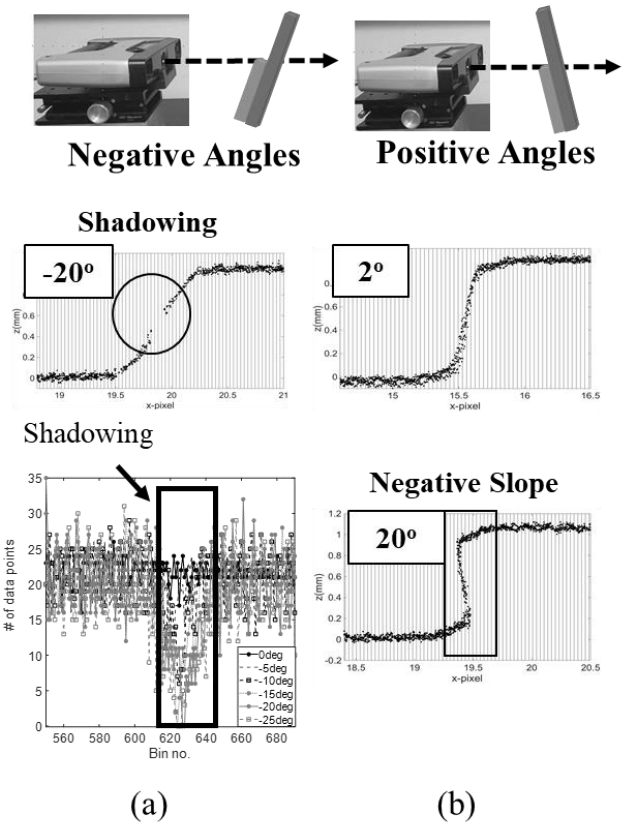

Fig. 2-8. (a) Tilt in the negative direction from the measurement axis leads to shadowing and appears as data drop out in the step profile. (b) Tilt in the positive direction leads to an undercut step profile.

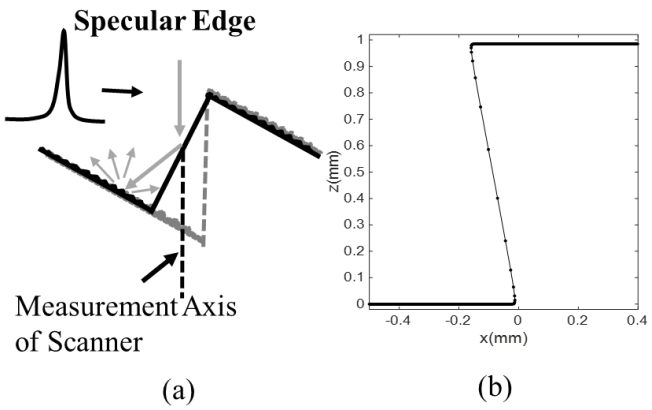

Fig. 2-9. (a) Incident light on a specular edge (black profile) is reflected, resulting in the mirror image of the diffuse surface to the left (dashed gray profile). (b) An undercut step profile results after completing the coordinate transformation data processing step.

2.4.2 Measurement conditions

Measurement conditions such as focus, location of the step in the field of view, and the angle alignment relative to the measurement axis - even with a diffuse-edge step artifact – are important influence factors to consider. This section covers the impact of these measurement conditions on the resulting ITF.

2.4.2.1 Focus condition

The artifact should be well focused for a good ITF measurement. The focus condition becomes more important for an instrument like the EinScan Pro which does not have a particular manufacturer-quoted focus distance but rather a working distance range (350 – 450 mm) is specified [15], as measured from the outermost mechanical surface on the measurement side of the EinScan. To assess the focus dependence, we varied the artifact position over the working distance from 350 mm to 450 mm in steps of 10 mm and measure the ITF at each position. The measured ITF at 380 mm is shown in the inset of Fig. 2-10, showing a 50% cutoff frequency of approximately 2.6 mm^{-1}. The measured variation over 350 mm to 450 mm is summarized in Fig. 2-10 with a graph of the resulting 50% ITF cutoff frequency as a function of position. The best resolution (highest cutoff frequency) occurs

at ~380 mm with a symmetric falloff with the position on either side. As expected, the ITF (spatial resolution) varies over the working distance. This highlights the importance of clearly specifying the position along the measurement axis (focus condition) of the ITF measurand (defined as position 380 mm ± 10 mm, in our case), and subsequently appreciating that the resolution of a scanned measurement result will vary over the 3D geometry of a part if there is appreciable depth variation to the part. The horizontal error bars in the figure are due to the estimated standard uncertainty in the distance measurement while the vertical error bars are the combined uncertainty of the cutoff frequency in the ITF measurements which is dominated by repeatability and the uncertainty due to the step angle calculation (describe in section 2.4.5.1).

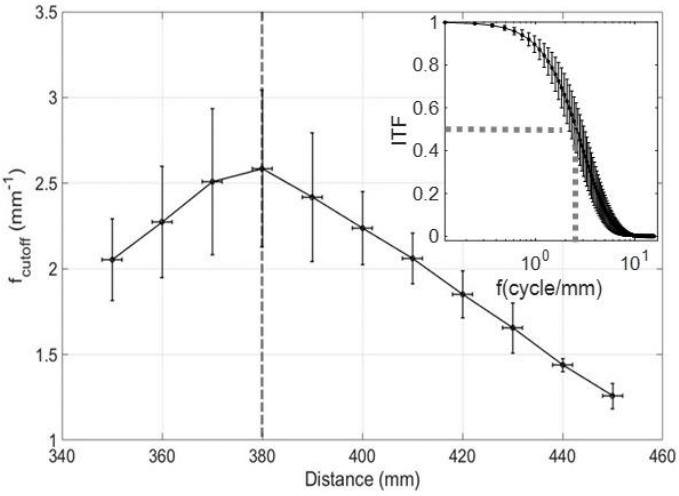

Fig. 2-10. The 50% cutoff value of the ITF as a function of the artifact position along the measurement axis shows the best resolution is at 380mm.

2.4.2.2 Position of the artifact in the field of view

The ITF varies over the measurement volume, with the best resolution occurring at best focus along the measurement axis and centered in *x* and *y* on the measurement axis (see Fig. 2-3). The sensitivity of the ITF to lateral positioning uncertainty must also be considered. We test this by changing the position of the artifact right/left and up/down (the

x and *y* axes) in the field of view at 400mm along the measurement axis (see Fig. 2-11(a)), moving the artifact to 25 mm to left, 7 mm to right, 22 mm to up, and 8 mm down. The ITF curves for these positions are shown in Fig. 2-11(b). The error bars are the combined uncertainty in the ITF measurements which is dominated by repeatability and the uncertainty due to the step angle calculation (describe in section 2.4.5.1). As we will see, even these relatively large *x/y* offsets lead to small ITF variation on the scale of the final combined uncertainty. We conclude for the EinScan then, that the lateral positioning uncertainty contribution is negligible as long as the step is positioned laterally within ± 10 mm of the measurement axis.

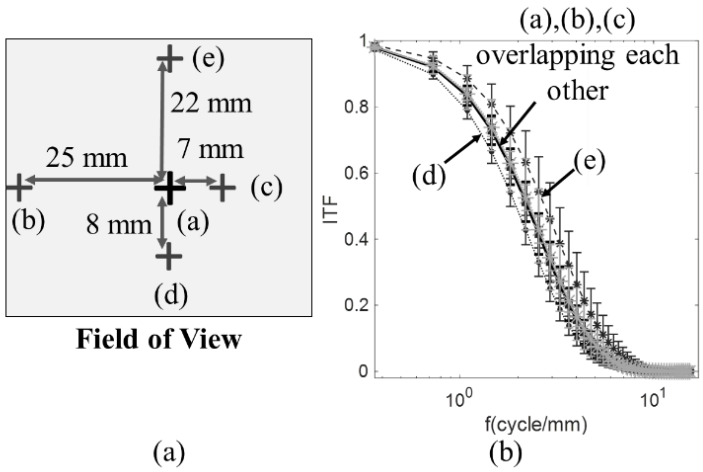

Fig. 2-11. (a) Location of artifact around the center of the FOV at 400 mm and (b) The ITF at different positions around the center of the FOV at best focus.

2.4.2.3 Measurement axis alignment (projection angle) condition

In section 2.4.1.2, we discussed the importance of the artifact alignment with the measurement axis (the projection angle) when the step has a specular edge. In this section, we show that the projection angle is important even when the step edge is diffuse. This is explored with simulation. With diffuse characteristics over the full step profile, the incident light scatters in all directions, thus the measurement becomes a direct mapping of

the angled profile along the measurement axis, then convolved with the LSF. For negative projection angles, the same behavior is expected as discussed in section 2.4.1.2. With a diffuse edge to the step, the positive projection angles now behave differently.

We simulate the same positive angle positions as in section 2.4.1.2 from 0^o to $+15^o$ in steps of 5^o and also at $+2^o$. We again use a 0.16-mm Gaussian LSF for the convolution (a model of the best-case resolution condition for the instrument). After the convolution, the 1D profile is rotated back to horizontal relative to the measurement axis to match what is done in the experiment. Once rotated back to horizontal, the step profile is deceptive because of the angle misalignment, leading to an artificially better ITF curve, as shown in Fig. 2-12. We can understand this trend as a simple projection of the LSF onto a measurement plane at an angle to the horizontal with a cosine dependence in essence, the LSF is effectively compressed by this factor, leading to apparently improved spatial resolution. The inset in Fig. 2-12(b) shows the comparison of the simulated ITF curve for the +15° misalignment and a simple convolution of a perfect step with a Gaussian LSF with a FWHM 0.16 mm reduced by a factor of cos (15°). Consideration of this effect leads to We conclude for the EinScan then, that the projection angle uncertainty contribution is negligible as long as the step is aligned +1° ± 1° relative to the measurement axis.

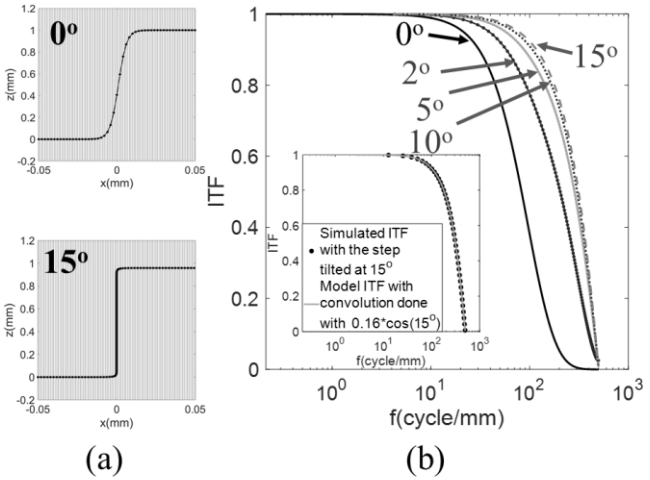

Fig. 2-12. (a) The simulated step profiles at zero and +15° show how the apparent corner curvature varies with misalignment angle, and (b) the ITF results show the ITF is lowest at 0° and highest at 15°

2.4.2.4 Orientation of artifact in FOV

We also explored the sensitivity of the measurement to the orientation of the step in the field of view (rotation about the measurement axis). The EinScan uses two cameras, positioned at slight angles on either side of the projection (measurement) axis in a horizontal plane. This configuration breaks the rotational symmetry about the measurement axis; therefore, the measurement could be sensitive to the step orientation relative to the plane of the cameras and projector. The orientations considered are shown on the left in Fig. 2-13 with the resulting ITF curves on the right. The error bars are the estimated combined uncertainties for the ITF measurements. The orientation of the fringes compared to the step orientation is conveyed by the overlay of black lines (fringes) on the left. The data shows with our current level of uncertainty ITF is independent of the step orientation.

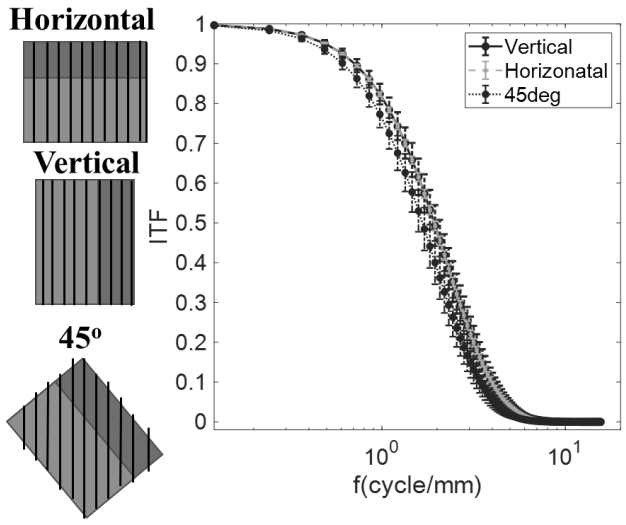

Fig. 2-13. The ITF at different rotation orientations at the 400 mm in the middle of the FOV.

2.4.3 Environment factors

The measurand can be affected by uncontrollable and small environmental changes such as mechanical vibration and/or electronic noise. We consider these environmental influence factors as causing random, zero-average, short-term variation in the measurand and therefore will be covered by experimental repeatability [23]. The results of the repeatability test are discussed in section 2.4.6.

2.4.4 Coordinate Transformation

A coordinate transformation is the very first data processing step, where we transform the data from a global coordinate system of the instrument to a local coordinate system on the point-cloud data (For detail see [3]). This involves choices in defining an origin and orientation for the local coordinate system and this will influence the ITF results. We divide the coordinate transformation into two parts: 1) masking the lower terrace that defines the local coordinate system orientation and 2) the choice of the local coordinate system origin. Masking is used to extract the points belonging to the lower terrace for use with a best-fit plane calculation to determine the orientation of the step artifact. We then choose one of

the points to define a local origin on the lower terrace, finally rotating the whole data set to this local coordinate system is done to remove the tip/tilt from the data. Both of these influences are covered in the repeatability assessment because they are also intrinsically random as the measurement and data processing are repeated.

2.4.5 Calculation of average step profile

The same average-profile data processing is carried out as is done for MTF measurements, as described in the ISO standard [24,25]. The step is measured at a slight orientation angle about the measurement axes, the data is then rotated about the measurement axes then to align the step vertically in the local coordinate system, and finally resampled and averaged to collapse the data to a single line profile estimate. We divide the average step profile calculation into two parts 1) angle calculation and 2) choice of the resampling interval.

2.4.5.1 Angle Calculation

After the coordinate transformation, we align the edge of the step artifact parallel to the y-axis of the local coordinate system and this requires an estimate of the angle for the rotation. The step angle estimate ends up being a dominant uncertainty contribution for our measurements. We use the same method to estimate the rotation angle as described in reference 13. In essence, an incorrect choice of angle leads to an artificially broad average line profile with a correspondingly poor ITF. The broadened line profile consequently has a large slope at the step transition. We estimate the best rotation angle by systematically varying the rotation angle through a range of values near the best angle, and plot the slope of the step transition region as a function of the rotation angle. A quadratic fit helps to estimate the optimum angle and it is $12.9^{o} \pm 0.2^{o}$ for our measurements. We estimate the

corresponding ITF uncertainty by repeating the ITF calculation using 12.7° and 13.1°, respectively, and then take the average of this change.

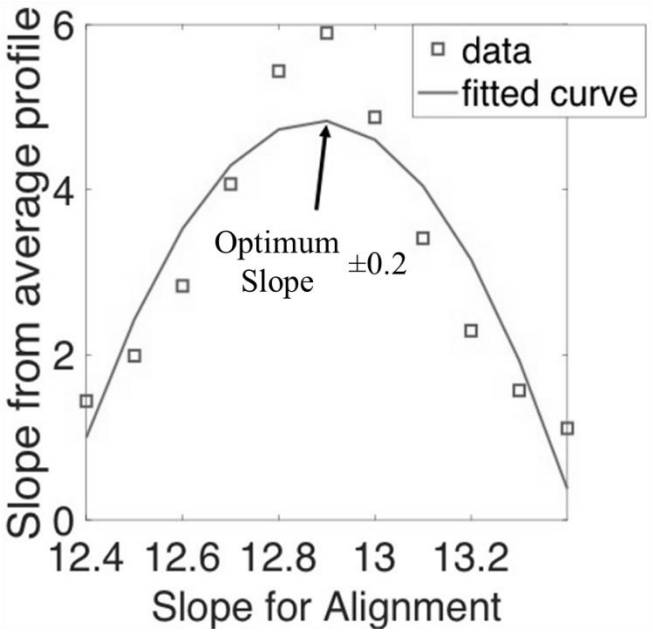

Fig. 2-14. Slope comparison approach for the uncertainty calculations due to the choice of the process parameter (angle calculation)

2.4.5.2 Resampling interval

Once the step profile has been aligned to the y-axis, it is collapsed and averaged to a single profile with the choice of a resampling interval. Too coarse of a resampling interval will filter the profile and lead to an ITF that reflects the resampling size rather than the bandwidth of the instrument. The resampling interval should be fine enough so the interval size choice does not affect the final ITF estimate. The resampling intervals considered were the EinScan reported point spacing of $\triangle x = 0.16$ mm and a range of smaller intervals: $\triangle x$, $\triangle x/2$, $\triangle x/3$, $\triangle x/4$, $\triangle x/5$, $\triangle x/6$, $\triangle x/7$, and $\triangle x/8$, where $\triangle x$ is the point spacing. The corresponding ITF curves are shown in Fig. 2-15. The curves become indistinguishable with a resampling interval of $\triangle x/4$ and finer. We use $\triangle x/5$ as the resampling interval for our data processing.

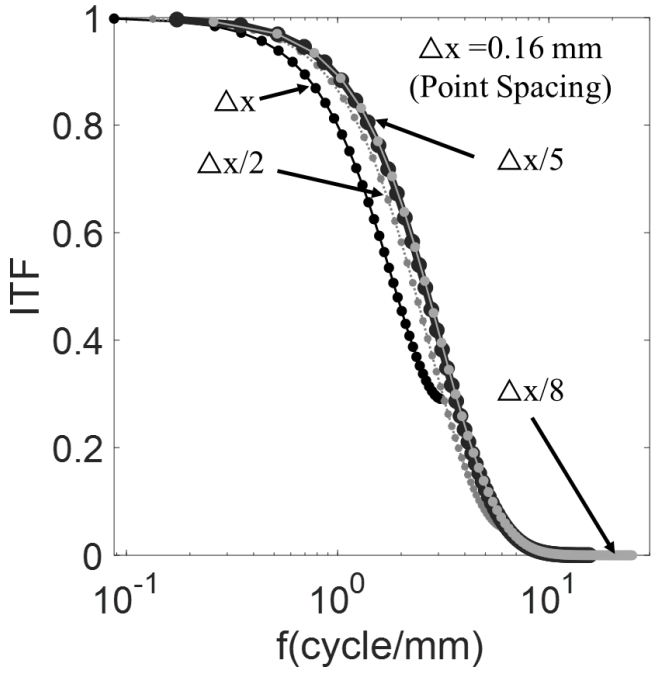

Fig. 2-15. The ITF for different resampling intervals

2.4.6 Repeatability

Repeatability is the variation in measurements taken by a single person or instrument on the same item, under the same conditions, and over a short time. A repeatability analysis will cover most of the uncertainties from our fishbone diagram, including uncertainty due to electrical noise, environment factors (short-term temperature variation and vibration, etc.), the masking and plane fit process, and the choice of the local coordinate system. To estimate repeatability, we repeat the ITF measurement ten times and take the average of the ten measurements as the best estimate of the ITF. The repeatability uncertainty, then, at each frequency value is the standard uncertainty in the mean which is the standard deviation of the ten values divided by $\sqrt{10}$ [23].

2.5 Measured ITF

As long as care is taken in the positioning and alignment of the step artifact, the combined uncertainty is dominated by repeatability and the uncertainty due to the step

rotation angle estimation. The combined uncertainty for ITF at each frequency is estimated by combining the standard uncertainty due to repeatability with the standard uncertainty estimated for the angle determination in a root-sum-square fashion.

The best estimate of ITF along with uncertainty (coverage factor = 2) at a working distance of 380 mm is shown in Fig. 2-16. The spatial frequency at which the ITF falls to 50%, the cutoff frequency, is 2.6 ± 0.5 mm^{-1}. The corresponding cutoff wavelength is around 0.38 ± 0.03 mm which is the estimate of the spatial resolution of the instrument. The comparison of this cutoff wavelength with the point spacing of 0.16 mm (manufacturer's metric to estimate resolution)) shows that the manufacture's quoted point spacing is an overly optimistic estimate of the resolution. The best possible ITF curve for the instrument, using the 0.16-mm FWHM Gaussian LSF is also shown in the figure for comparison. Interestingly the ITF predicted using the point spacing based LSF is a reasonable estimate of what we measured the ITF. Notice based on ISO standard the ITF predicts the 50% frequency cutoff 2.6 mm^{-1} which corresponds to a 50% cutoff wavelength of 0.38 mm which is approximately two times larger than the 0.16 mm point spacing, which would be a user's estimate of the resolution.

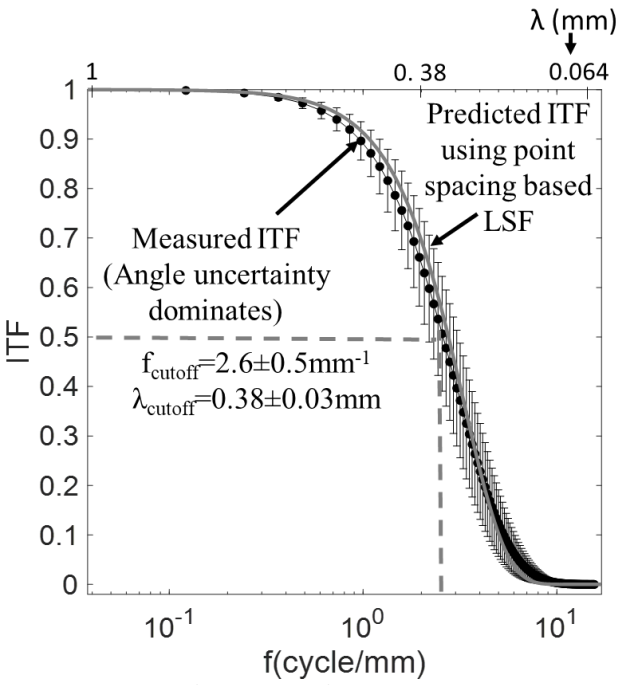

Fig. 2-16. The final estimate of the ITF with the uncertainty

2.6 Conclusion

Measurement of the ITF of a structured light system is presented and the different factors which can contribute to uncertainty have been discussed. Several factors must be considered carefully while taking the ITF measurement and processing the data. If care is taken with the alignment of the step artifact, the most important contributions to our uncertainty are the angle estimation to align the step edge parallel to the y-axis during data processing and repeatability. With respect to alignment, the angle of the artifact to the projection axis (the angle of the normal vector of either terrace of the step artifact to the measurement axis) is important. A negative tilt angle leads to the shadowing effect which appears as the data drop in both cases. Tilt in a positive direction will cause an apparent undercut in the step profile in the case of the specular edge step artifact whereas a diffuse edge leads to an artificially improved ITF estimate. This is purely a geometric projection effect. The importance of the focus condition along with the lateral position of the artifact

in the field of view has been discussed. The best focus for the EinScan Pro is found to be 380 ± 10 mm and the change in ITF is negligible within ± 10 mm lateral positioning around the measurement axis. The sensitivity of the ITF to the step orientation of the artifact within the field of view was also discussed, and the ITF was found to be not significantly affected by this measurement condition. The choice of the resampling interval was also explored. In addition, the characterization and validation methods for the step artifact were discussed.

REFERENCES

1. Xavier, C. d. L. and de Groot. P. J., “Lateral resolution and instrument transfer function as criteria for selecting surface metrology instruments,” Imaging and Applied Optics Technical Digest (Optical Society of America), OTu1D4 (2012).

2. de Groot, P., de Lega, X. C., de Lega, X. C., “Interpreting interferometric height measurements using the instrument transfer function,” Fringe 2005, 30–37 Springer Berlin Heidelberg, Berlin, Heidelberg (2006).

3. Jain, S., Zhang, B. and D. Allen, A., “Evaluation of the spatial frequency response and the uncertainty for a commercial structured light system,” Proc. of SPIE Vol. 11102 (2019).

4. der Jeught, S. V., and Joris, J. J. D., “Real-time structured light profilometry: a review,” Optics and Laser Engineering 87, 18-31(2016).

5. Gupta, M., Agrawal, A., Veeraraghavan, A. and Narasimhan S.G., “Structured light 3D scanning in presence of global illumination,” Proc. CVPR (IEEE) 2011, 713-720 (2011).

6. Tianquan, S., Maldonado, A., Su, P., Zhou, P. and Burge, J.H., “Study of the instrument transfer function of a free-form optics metrology system: SCOTS,” Proc. SPIE 9046, 904602-1-904602-7 (2013).

7. Tianquan, S., Maldonado, A., Su, P., Zhou, P. and Burge, J.H., “Instrument transfer function of slope measuring deflectometry systems,” Applied Optics (Optical Society of America) 54, 2981-2990 (2015).

8. Torsten Glaschke, Leslie L. Deck, and Peter J. de Groot "Characterizing the resolving power of laser Fizeau interferometers", Proc. SPIE 10829, Fifth European Seminar on Precision Optics Manufacturing, 1082905 (7 August 2018).

9. X. C. de Lega and P. J. de Groot, "Lateral resolution and instrument transfer function as criteria for selecting surface metrology instruments," in Imaging and Applied Optics Technical Papers, OSA Technical Digest (online) (Optical Society of America, 2012), paper OTu1D.4.

10. Kellner, T., Breitbarth, A., Zhang, C. and Notni, G., “Characterizing 3D sensors using the 3D modulation transfer function,” Measurement Science and Technology 29,1-8 (2018).

11. M. Goesele, C. Fuchs and H. -. Seidel, "Accuracy of 3D range scanners by measurement of the slanted edge modulation transfer function," Fourth International Conference on 3-D Digital Imaging and Modeling, 2003. 3DIM 2003. Proceedings., 2003, pp. 37-44, DOI: 10.1109/IM.2003.1240230.

12. Leach, R., Giusca, C., Henning, A., Sherlock, B. and Coupland, J., “ISO definition of resolution for surface topography measuring instruments,” Fringe 2013, 405-410 Springer (2014).

13. Bin Zhang, Angela Davies, Christopher Evans, and John Ziegert, "Validity of the instrument transfer function for fringe projection metrology," Appl. Opt. 57, 2795-2803 (2018).

14. Zhang, B., D. Allen, A., Ziegert, J., and Evans, C., “Application of instrument transfer function to a fringe projection system for measuring rough surfaces,” Proc. SPIE 10373, 103730S (2017).

15. Shinning 3D, “EinScan-Pro user manual”. (2018)

16. https://www.einscan.com/handheld-3d-scanner/einscan-pro-hd/ (July,18,2021)

17. Berssenbrügge, P., Dekiff, M., Kemper, B., Denz, C.., Dirksen, D., “Characterization of the 3D resolution of topometric sensors based on fringe and speckle pattern projection by a 3D transfer function,” Optics and Laser Engineering 50, 465–472 (2012).

18. Jiyoung Chu, Quandou Wang, John P. Lehan, Guangjun Gao, and Ulf Griesmann "Measuring the phase transfer function of a phase-shifting interferometer", Proc. SPIE 7064, Interferometry XIV: Applications, 70640C (11 August 2008).

19. B. Doerband and J. Hetzler "Characterizing lateral resolution of interferometers: the Height Transfer Function (HTF)", Proc. SPIE 5878, Advanced Characterization Techniques for Optics, Semiconductors, and Nanotechnologies II, 587806 (30 August 2005).

20. Daniel M. Sykora and Peter de Groot "Instantaneous measurement Fizeau interferometer with high spatial resolution", Proc. SPIE 8126, Optical Manufacturing and Testing IX, 812610 (27 September 2011).

21. L. L. Deck and P. J. de Groot, "Using the instrument transfer function to evaluate Fizeau interferometer performance," in Optical Design and Fabrication 2017

(Freeform, IODC, OFT), OSA Technical Digest (online) (Optical Society of America, 2017), paper OM2B.7.

22. Peter Z. Takacs, Michelle X.-O. Li, Karen Furenlid, and Eugene L. Church "Step-height standard for surface-profiler calibration", Proc. SPIE 1995, Optical Scattering: Applications, Measurement, and Theory II, (1 December 1993).

23. Bevington, P.R., Robinson, D.K., [Data Reduction and Error Analysis for The Physical Science Third Edition], Mc Graw Hill, (2003).

24. Reichenbach, S.E., Park, S.K. and Narayanswamy, R., "Characterizing digital acquisition devices," Optical Engineering 30, 170-177 (1991).

25. Masaoka, K., Yamashita, T., Nishida, Y. and Sugawara, M., "Modified slanted-edge method and multidirectional modulation transfer function estimation," Optics Express 22, 6040-6046 (2014).

Chapter 3. DETERMINATION OF NON-LINEARITY FOR 3D MEASUREMENTS

ABSTRACT

In recent years, the modulation transfer function (MTF) and the instrument transfer function (ITF) have become popular metrics to characterize imaging and three-dimensional topographical measurement resolution, respectively. However, MTF and ITF resolution classification are spatial frequency based and they rely on the assumption of measurement linearity. Therefore, an approach for detecting the degree of measurement nonlinearity is useful to validate these frequency-based resolution metrics. In this paper, we present a general methodology of identifying the degree of non-linearity which can be used for both the imaging systems and 3D topography instruments.

3.1 Introduction

Only for a linear system (or approximately linear system) can spatial-frequency-based metrics like the instrument transfer function (ITF) for topographic measurements and the modulation transfer function (MTF) for imaging systems be used as a sensible metric of spatial resolution [1-3]. Such measurements are only approximately linear in some limit, hence a method of checking the measurement for non-linearity is important for validating the resolution characterization. A system is linear if its response is the sum of the responses that each Fourier component signal would produce individually, i.e., if two frequency components are present in an input signal, we can propagate them separately and add up the result [3]. For example, for a linear system, the output of a sinusoidal input would be sinusoidal with a modified amplitude (see Fig. 3-1(a)). However, a non-linear system generates harmonics of the input frequency which modify the shape according to the type of non-linearity (see Fig. 3-1(b)) [4].

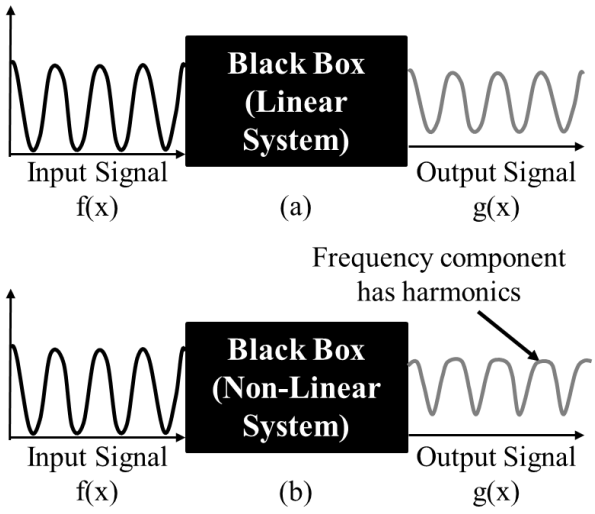

Fig. 3-1. (a) An example of a linear system and (b) an example of a non-linear system.

Imaging and 3D topographic measurements are linear in specific limits and these have been investigated and theoretically defined in the literature. Theoretical studies on interferometers have suggested that measurements are linear under the following two conditions [1,2,5-9]:

1. The optical system has a sufficiently large numerical aperture to capture the light scattered from the topography object, including the higher diffraction orders.
2. The size of a step or steep sidewall is much less than one quarter of the mean wavelength.

For a fringe projection system, the theory has been discussed showing that the system is linear if the surface height variation is small compared to the carrier wavelength and also much smaller than the working distance [4,10]. These considerations define practical regimes of linearity for traditional uses but are becoming increasingly challenged by applications involving complex textures and high surface slopes [11]. Only a few

publications are in the literature about non-linear analysis for imaging systems such as infrared imaging and detector array. Becherb, et al. determined the non-linearity of the optical imaging system in terms of the ratio of the coherence interval of the object illumination to the size of the imaging system's diffraction pattern and showed that imaging systems are linear as long as this ratio is less than 1 [12]. Orlando, et al. used a gamma correction method to remove the non-linearity of a forward-looking infrared system (FLIR) [13]. Boreman, et al. used a piecewise linear algorithm on each pixel for correcting the non-linearity of a HgCdTe IR CCD focal plane [15] and later on presented the use of spatial distortion test (Fourier analysis) for characterization of the non-linearity of a CID camera and vidicon tube camera [15]. For 3D topography measurements, approaches to detecting the presence of nonlinearity have not been addressed. Non-linearity will lead to incorrect MTF/ITF results and further, the MTF/ITF results will depend on the particular artifact used for the resolution characterization [12,16].

In this paper, we present a general methodology through theory and simulation to determine whether a measurement is linear. The methodology can be applied to any topographic or optical imaging instrument. One aspect of the approach leverages the concept of the coherence function from the mechanical structure dynamics to check for non-linearity in the system. This works for individual sinusoidal inputs but does not work for step-based artifacts which are commonly used to measure the MTF of imaging systems and the ITF of topographic instruments. We then present the use of a higher-order spectral function - the bispectrum - for non-linearity determination which works on both a sinusoidal and step input.

3.2 Coherence Function

The coherence function measures the degree of mutual coherence or the likeness of two harmonic signals [17-20]. The coherence function is widely used in system identification, measurement of the signal to noise ratio, determination of linearity and non-linearity of the system, and the determination of time delay [17-20]. Most of the applications are for the signal is time-frequency based, but our application is instead spatial frequency based. Whether time or spatial frequency based, the output *g(x)* (using spatial-frequency-based here) can be written as the convolution of the input *f(x)* and the frequency response function *h(x)*:

$$g(x) = f(x) \otimes h(x) \tag{2.1}$$

In the Fourier domain,

$$G(f) = F(f).H(f) \tag{2.2}$$

where, *G(f)*, *F(f)*, and *H(f)* are the Fourier transforms of *g(x)*, *f(x)*, and *h(x)*, respectively. The function *H(f)* is called the frequency response or instrument transfer function.

The coherence function between two functions *f(x)* and *g(x)* is defined as the cross-power spectrum $S_{fg}(f)$ divided by the square root of the product of two power spectrum $S_{ff}(f)$ and $S_{gg}(f)$ [17-24].

$$\gamma_{fg}^2(f) = \frac{S_{fg}(f)}{\sqrt{S_{ff}(f)S_{gg}(f)}}. \tag{2.3}$$

where, $S_{fg}(f)$ is the cross-power spectrum defined as:

$$S_{fg}(f) = F^*(f)G(f), \tag{2.4}$$

$S_{ff}(f)$ and $S_{gg}(f)$ is the auto-power spectrum defined as

$$S_{ff} = F(f)F^{*}(f), \tag{2.5}$$

And

$$S_{gg}(f) = G(f)G^{*}(f), \tag{2.6}$$

where, $F^{*}(x)$ and $G^{*}(x)$ are the complex conjugate of the Fourier transform of the $f(x)$ *and* $g(x)$ respectively.

The coherence function is a normalized cross-spectral density function that can be used as a measure of the spectral similarity between two signals. The coherence function characterizes energy conservation. The value of the coherence function lies within 0 and 1. If a system is linear and in absence of noise energy is conserved and coherence is 1. The coherence function is sensitive to noise and system non-linearity which causes its value to be less than 1. However, two completely uncorrelated signals cause the coherence value to be 0 [17-24].

3.2.1 Use of the coherence function for determination of non-linearity with sinusoidal waves

MTF/ITF both can be measured using a sine wave pattern or a step artifact [12,13,16,25], the only difference is that amplitude is the height for ITF and intensity for MTF measurements. We test the capability of the coherence function in both cases. Extending what has been done with the coherence function in the time domain [17,18,24], we applied the approach in the spatial domain by starting with a sinusoidal function, we create a linear input function which is the sum of two sine waves with frequencies of 25mm^{-}

^{1} and 100mm^{-1} And create a non-linear output which has non-linear interaction between the frequencies of the input signal, i.e., for the input,

$$I(x) = A_0 + A_1 \sin(2\pi f_1 x) + A_2 \sin(2\pi f_2 x) \tag{2.7}$$

The nonlinear output is given by

$$\begin{aligned} O(x) = k[&A_0 + A_1 \sin(2\pi f_1 x) + A_2 \sin(2\pi f_2 x) + A_3 \sin(2\pi f_3 x) \\ &+ A_4 \sin(2\pi f_4 x) + A_5 \sin(2\pi f_5 x) + A_6 \sin(2\pi f_6 x)) \end{aligned} \tag{2.8}$$

where, f_1 =25 mm^{-1} and f_2=100 mm^{-1}, f_3 is the sum of the frequencies $f_3=f_1+f_2$=125 mm^{-1}, f_4 is the difference if the frequencies, $f_4=f_2-f_1$=75 mm^{-1}, f_5 and f_6 are the double frequencies, $f_5=2f_1$=50 mm^{-1}, and $f_6=2f_2$=200 mm^{-1}. A zoomed view of both waves is shown in Fig. 3-2.

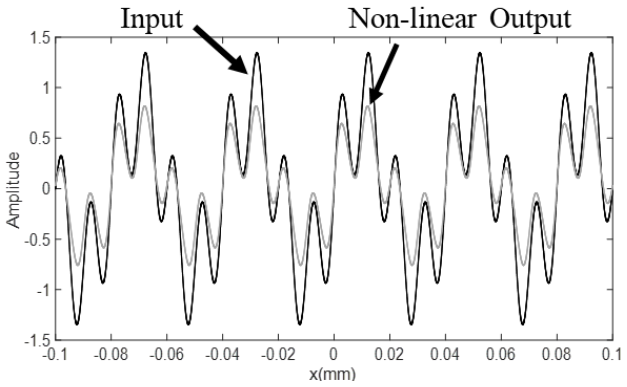

Fig. 3-2. Input and output sinusoidal signals with input having the frequencies of 25mm^{-1} and 100mm^{-1} and the output signal contains additional harmonics of sum frequency 125mm^{-1}, the difference of frequency 75mm-^{1}, and double frequencies of 50mm^{-1} and 200mm^{-1}

Now, we calculate the coherence between two waves and since the coherence measures the likeness of the two signals, we expect the coherence to be 1 everywhere except at f_3=125 mm^{-1}, f_4=75 mm^{-1}, f_5=50 mm^{-1}, and f_6=200 mm^{-1} and the result agrees with our prediction shown in Fig. 3-3. (A zoomed view is shown in the inset of Fig. 3-3).

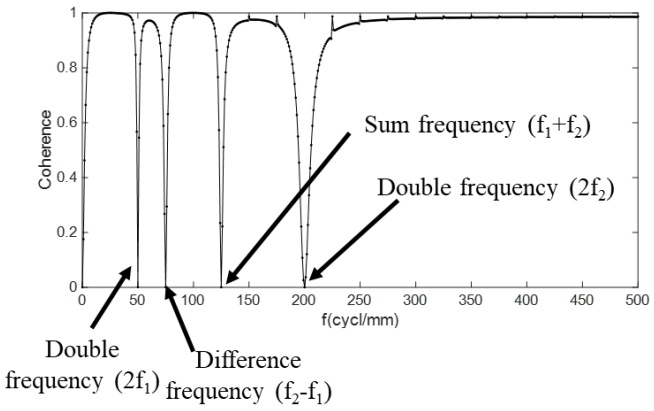

Figure 3-3. The coherence function calculated for a sinewave shows the presence of the harmonics.

3.2.2 Failure of the coherence function for determination of non-linearity with a step artifact

Now through simulation, we applied the coherence function calculations on a step artifact. We first create a perfect step profile then convolve this profile to a Gaussian LSF. Then duplicate the convolved step and then duplicate the step 1000 times to generate a long signal input. Then we create a nonlinear output by applying a quadratic nonlinearity to the input. A zoomed view of both the input and output is shown in Fig. 3-4(a). The types of nonlinearity would be system dependent and an arbitrary 2^{nd} order nonlinearity is used here for demonstration purposes. Regardless of the nonlinearity used, the coherence function value is one over the whole frequency range (Fig. 3-4(b)). This is because the input signal has infinite frequency content. The coherence calculation detects the presence of nonlinearity by highlighting frequencies that should not be in the output, but this fails when all frequencies exist in the input and the output, regardless of the linearity condition. Thus, a different analysis is needed when a step artifact is used, or any infinite-frequency-content artifact, for that matter.

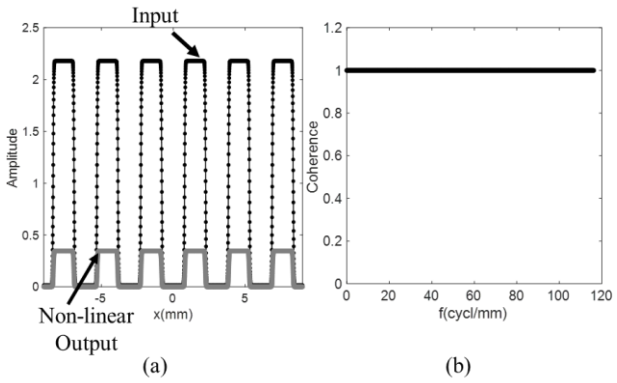

Fig. 3-4. (a) Input and a non-linear output, and (b) The coherence function for a step function is one over the whole frequency range

3.3 The Bispectrum

Higher-order spectral analysis (HOSA) techniques can be used to identify the degree of non-linearity, the presence of non-Gaussian random processes, and phase coupling in wave interactions [26-29]. The high order spectra (HOS) are defined in terms of high order cumulants or moments of the random processes. The bispectrum is a third order spectrum and highlights information about the quadratic interaction and the phase coupling between two signals [26-32]. The bispectrum techniques for noise reduction and detection of quadratic non-linear phase coupling have been applied in several fields like astronomy [26,28], geographical [26 ,28], communication engineering [32], biomedical [32], electrical [26, 29, 32], mechanical [26, 29, 32], and interferometry [32], oceanography [28,29], coupled fluid mechanical [26,28], image processing [32,33] and plasma density fluctuation [28,29].

The bispectrum is defined as the Fourier transfer of the third order cumulant or moment of a stationary process [26-34]. For a stationary signal with zero mean, the third order cumulant is the same as the moment and is defined as

$$C(k,l) = E\{x(i)x(i+k)x(i+l)\} \tag{2.9}$$

where *x* is the value at index i, and k and l are shifted indices. The operator E{} is the expectation operation.

The bispectrum is the Fourier transform of this function and is given by

$$B(p,q)=\sum_{l=0}^{N-1}\sum_{k=0}^{N-1}C(l,k)\exp(-j2\pi(pl+qk))=F\{C(l,k)\} \tag{2.10}$$

where, N is the length of the signal and F{} represents the Fourier transform.

For simplicity and a real discrete signal [32], we can write equation (9) as

$$B(p,q)=X(p)X(q)X(-p-q) \tag{2.11}$$

where, p and q are indices in the bispectrum domain and range from -N/2+1 to N/2-1. The term X() is the Fourier transform operator.

The bispectrum has some useful properties [26,30-33]:

1. For a stationary Gaussian signal with zero mean, the bispectrum is zero. Thus, the bispectrum removes or reduces the noise from a signal contaminated with zero mean Gaussian noise.
2. A temporal or spatial shift does not affect the bispectrum.
3. The bispectrum retains the phase and amplitude of the Fourier transform of the signal, which is not the case with the power spectrum calculation.
4. If there exist three frequencies within a signal, where the sum of the two frequencies appears in the third frequency, then a non-zero value will appear in the bispectrum.

The 4th property is the most important for our application. Using this property one can identify the quadratic nonlinear interaction of the harmonic input components and hence identify the presence of non-linearity.

3.3.1 Use of the bispectrum for determination of non-linearity with sinusoidal waves

First, to highlight the features of a bispectrum calculation, we follow what has been demonstrated [37] in the literature but instead of the time domain we use the spatial domain and apply the bispectrum to a simple 2-frequency content signal [28-30,36]. We create two signals, signal 1 with frequency f_1=25 mm^{-1} and signal 2 with frequency f_2=2f_1=50 mm^{-1} (Fig. 3-5(a)). We then sum the two to create a single signal having frequency f_1 and 2 f_1 (double frequency), followed by the addition of significant random noise having a standard deviation of 10 times the amplitude of the frequencies. The final signal with the noise is shown in Fig. 3-5(b). We calculate the Fourier transform of the signal to check if the Fourier transform can identify the presence of both frequencies (Fig. 3-6) and we see that the Fourier transform fails to identify the existing frequencies in the signal when data is noisy.

The bispectrum has the advantage over the Fourier transform and the coherence function as the bispectrum of Gaussian noise is zero and spreads the noise over a 2-dimensional plane. This reduces the impact of the noise and makes it easier to identify the frequency for which the double (or the sum) frequency exists A line profile along the diagonal i.e., along the line where $f_1 = f_2$ is shown in Fig. 3-7. The bispectrum plot is shown as an inset in Fig. 3-7 showing the existence of the quadratic non-linearity by having a clear peak at $f_1 = f_2$ =20 mm^{-1}. The bispectrum is more helpful than a coherence function calculation, even for harmonic signals because the coherence function, unlike the bispectrum, is sensitive to

noise and causes an overall reduction in the coherence value, complicating the interpretation of the result.

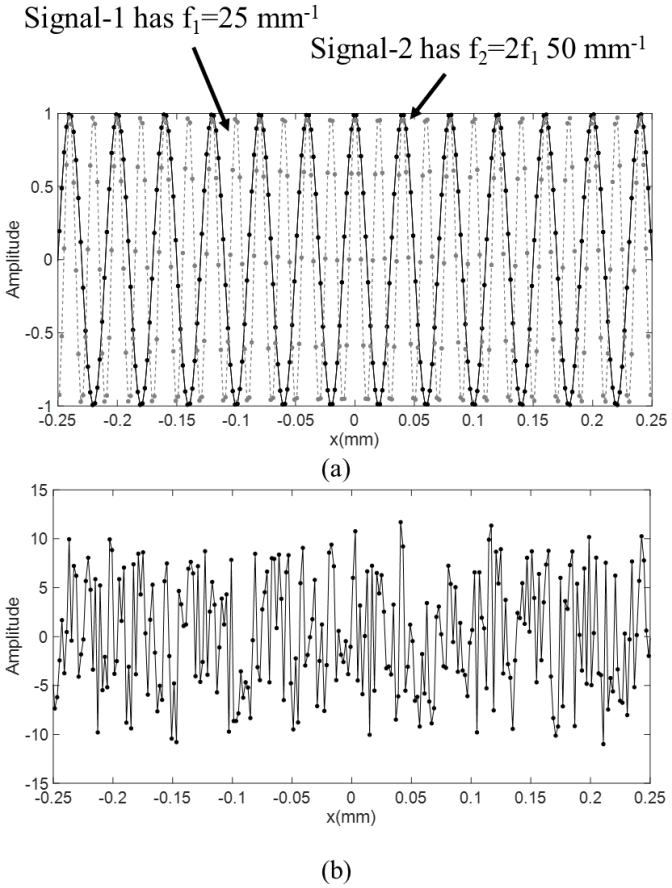

Fig. 3-5. (a) Two signals before adding noise having different frequencies of 25mm^{-1} and 50 mm^{-1}, and (b) Total Signal sum of the two signals in (a) plus a random noise with a standard deviation of 20.

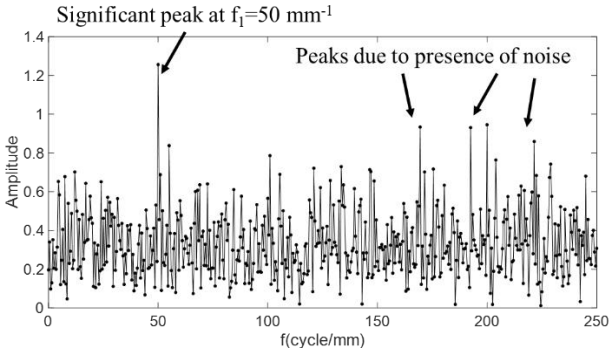

Fig. 3-6. The Fourier transform of sinewave in Fig. 1(b) shows the difficulty to recognize the presence of inherent frequency in the signal due to noise.

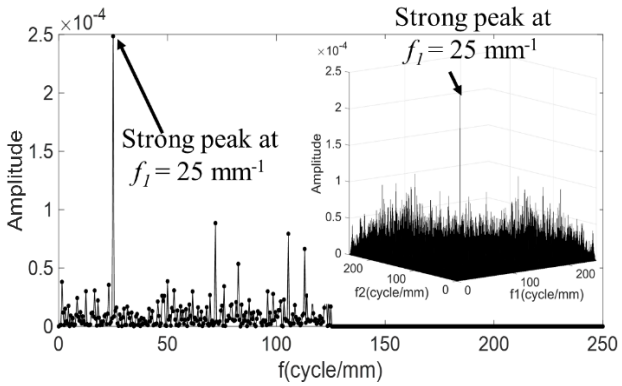

Fig. 3-7. A line profile along the line f_1=f_2 (along diagonal), and the bispectrum show a strong peak at f_1=25mm^{-1}, confirming the existence of 2f_1=50mm-1 in the signal.

3.3.2 Use of the bispectrum to determine the non-linearity with a step artifact

Through simulation, we applied the bispectrum calculation to a step artifact with and without noise to investigate the bispectrum analysis when a step artifact is used for the input. We apply a non-linearity to the output that is similar to what is observed for optical detector nonlinearity in cameras. Both cases are summarized below.

3.3.2.1 Bispectrum with no noise added to the input function

The bispectrum detects the presence of the double frequency in a signal. A step artifact has an infinite frequency content with a well-defined amplitude dependence on frequency. Consequently, a double frequency exists for all frequencies in the input. However, if the output is linear, the ratio of each frequency's amplitude to the amplitude of 2f is well-defined. Detection of nonlinearity, then, can be highlighted by comparing a bispectrum calculation for a linear step output compared to a nonlinear step output. To test this, we create a rect function (amplitude≈0.5) and convolve it with a Gaussian line spread function (LSF). To add non-linearity, we use a response curve measured for a DSLR camera shown in Fig. 3-8 where the output falls below the linear response curve with increasing intensity (slope = 1). In the case of a real image-system-based experiment, we would be comparing

the results from the linear region (low intensity) and the non-linear region (high intensity). Thus, in the simulation, we create another perfect step with an amplitude approximately equal to 1.4 greater than the linear step (to reflect the use of the higher nonlinear intensity level), convolve this step with the LSF, and then apply the nonlinearity using the fit to the curve in Fig. 3-8. The comparison of both linear and non-linear signals along with the amplitudes picked from the linear and non-linear region is shown in Fig. 3-8.

Now the bispectrum was calculated for both the linear output and the non-linear output. The important step here is to normalize the bispectrum by the area under the curve for comparison. The bispectrum is not inherently normalized. Both the linear and the non-linear bispectrum were normalized by dividing by the area under the 2D bispectrum curve, respectively. The normalized 2D bispectrum linear step artifact output is shown in Fig. 3-9 and the profile along the diagonal is shown in Fig. 3-10. The two notable features in the line profile correlate to the frequency signatures of the width of the LSF and half the width of the LSF as labeled in the figure. of the linear and nonlinear comparison shows that the bispectrum along the diagonal of a non-linear step signal is higher in the mid-spatial frequency region than that of the linear signal. We further see the presence of the non-linearity in the 2D bispectrum space by plotting the difference between the normalized linear and non-linear bi spectra as shown in the inset in Fig. 3-10.

It is important to note that in practice if only a single artifact is experimentally used to measure the frequency response of the system, the ability to use this technique to check for nonlinearity is limited. Knowledge of the line spread function of the system in the linear limit is needed to generate a simulated linear bispectrum for the comparison. Naturally a step artifact with as large of a step as possible is desirable (whether actual height for

assessing topographic instrument or intensity for optical systems) because this generates a larger signal-to-noise MTF or ITF measurement. But the use of an artifact with a large step amplitude runs the risk of crossing over into the nonlinear response limit. The best approach would be to measure a second artifact that is clearly in the theoretical linear limit of the measurement and use this measurement to generate the normalized linear bispectrum for the difference assessment.

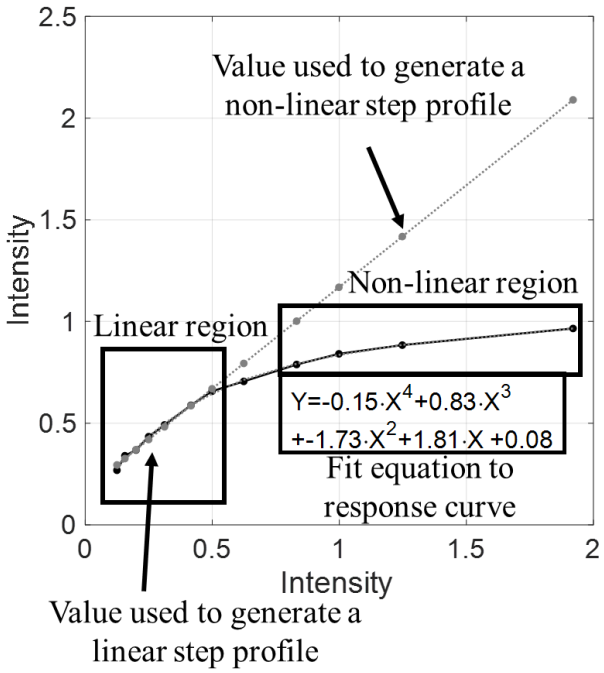

Fig. 3-8. A linear camera model is shown in gray, and a non-linearity response curve in black, showing the linear response at low intensity and the nonlinear response with increasing intensity input due to camera saturation. The fir to the non-linear response curve if a 4th order degree polynomial.

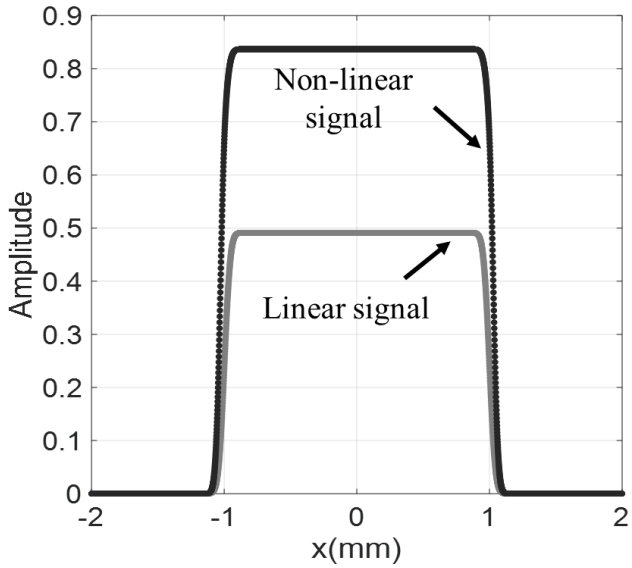

Fig. 3-9. A comparison of linear (gray curve) and non-linear (black curve) steps.

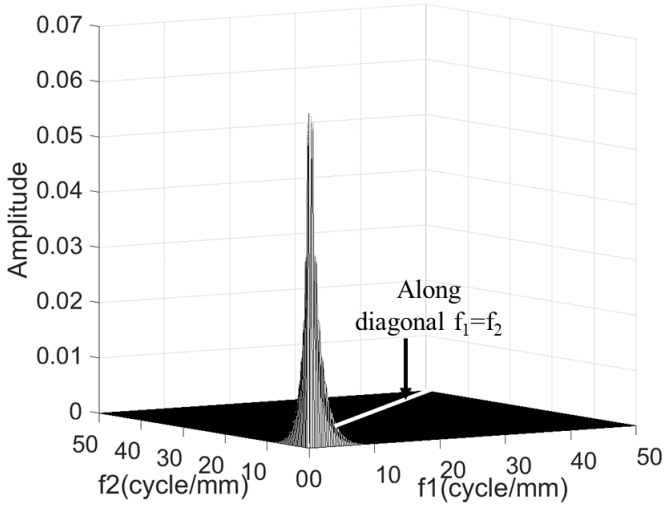

Fig. 3-10. The normalized bispectrum of the linear step.

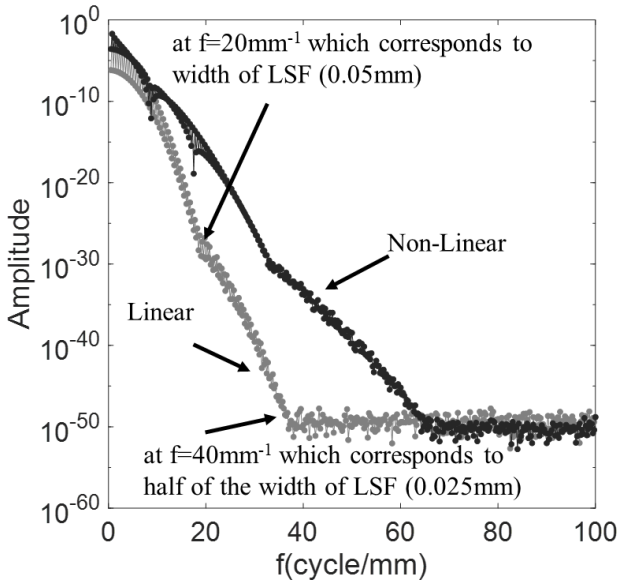

Fig. 3-11. A line profile along diagonal showing the bispectrum of a non-linear step is higher than that of a linear step function.

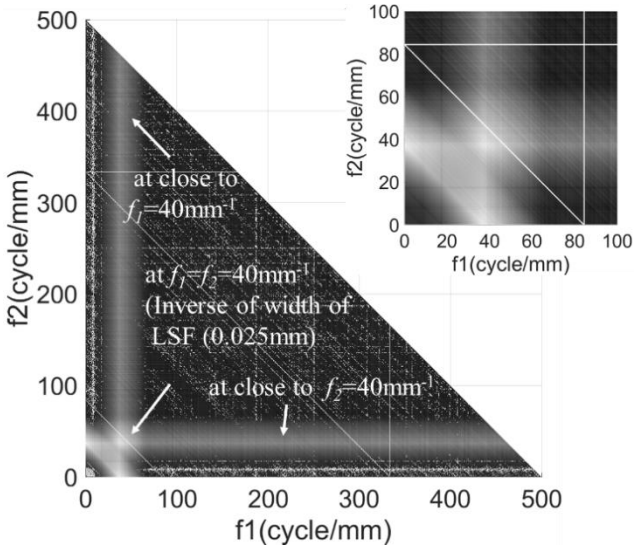

Fig. 3-12. The subtraction of non-linear and linear bispectrum showing the presence of non-linearity. Inset shows the zoomed view from f=0 mm-1 to 100 mm-1 showing a significant sign of non-linearity.

3.3.2.2 Use of the bispectrum with the addition of noise

A random noise of standard deviation of 0.02% of step height of nonlinear step and 0.04% of step height of linear step were added to both the linear and the non-linear steps from Fig. 3-9 respectively. Then the normalized bispectra were calculated and subtracted. The comparison of the line profile along the $f_1=f_2$ (the diagonal) is shown in Fig. 3-13 and

the difference of the both linear and the non-linear bispectrum as an inset is shown in Fig. 13 and

The difference between the linear and nonlinear behavior is impacted by the noise, but a difference is still observable. Simulations over a range of noise levels would guide experimental choices on the signal to noise level needed to detect the nonlinearity.

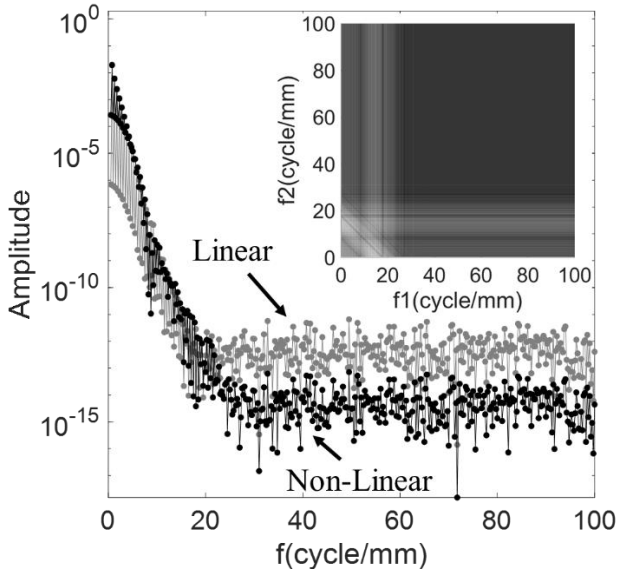

Fig. 3-13. A line profile along diagonal showing the bispectrum of a non-linear step is higher than that of a linear step function when a random noise is added, and the subtraction of non-linear and linear bispectrum when noise is added. The presence of non-linearity is still detectable. Inset shows the zoomed view from f=0 mm^{-1} to 100 mm^{-1} showing a significant sign of non-linearity.

3.4 Conclusion

The identification of non-linearity when characterizing the spatial frequency response of 3D topography measurements (called the instrument transfer function ITF) or imaging systems (called the modulation transfer function MTF) was discussed. We propose the use of the coherence function and the bispectrum calculation to test for nonlinearity. Through simulation, both methods were applied to the most commonly used artifact for these measurements, namely a step artifact. The bispectrum calculation has the advantage over the coherence function as it can be used both for the traditional step artifact and for sinusoidal artifacts, whereas the coherence calculation is only useful when using a

sinusoidal artifact. Even when using a sinusoidal artifact where the coherence calculation highlights the nonlinearity, it is also strongly impacted by noise, potentially obscuring the non-linearity. However, the noise reduction property of the bispectrum results in a clearer detection of nonlinearity alone. This feature also makes the bispectrum analysis advantageous over a traditional Fourier approach. One could consider even higher order spectral analyses like the tri-spectrum. Evan with the bispectrum analysis, noise degrades the ability to detect the nonlinearity, necessitating a consideration of desired experimental signal-to-noise levels to achieve a useful nonlinearity assessment.

REFERENCES

1. Leach R., Giusca C., Henning A., Sherlock B., Coupland J. (2014), " ISO Definition of Resolution for Surface Topography Measuring Instruments," In: Osten W. (eds) Fringe 2013. Springer, Berlin, Heidelberg.

2. de Groot P., de Lega X.C. (2006)," Interpreting interferometric height measurements using the instrument transfer function," In: Osten W. (eds) Fringe 2005. Springer, Berlin, Heidelberg.

3. Bin Zhang, Angela Davies, Christopher Evans, and John Ziegert, "Validity of the instrument transfer function for fringe projection metrology," Appl. Opt. 57, 2795-2803 (2018).

4. Glenn D. Boreman, Anthony B. Centore, and Christopher R. Costanzo "Spatial harmonic distortion: a test for focal plane nonlinearity," *Optical Engineering* 30(5), (1 May 1991).

5. Tianquan Su, Alejandro Maldonado, Peng Su, and James H. Burge, "Instrument transfer function of slope measuring deflectometry systems," Appl. Opt. 54, 2981-2990 (2015).

6. Torsten Glaschke, Leslie L. Deck, and Peter J. de Groot "Characterizing the resolving power of laser Fizeau interferometers", Proc. SPIE 10829, Fifth European Seminar on Precision Optics Manufacturing, 1082905 (7 August 2018).

7. X. C. de Lega and P. J. de Groot, "Lateral resolution and instrument transfer function as criteria for selecting surface metrology instruments," in *Imaging and Applied Optics*

Technical Papers, OSA Technical Digest (online) (Optical Society of America, 2012), paper OTu1D.4.

8. Daniel M. Sykora and Peter de Groot "Instantaneous measurement Fizeau interferometer with high spatial resolution", Proc. SPIE 8126, Optical Manufacturing and Testing IX, 812610 (27 September 2011).

9. L. L. Deck and P. J. de Groot, "Using the instrument transfer function to evaluate Fizeau interferometer performance," in *Optical Design and Fabrication 2017 (Freeform, IODC, OFT)*, OSA Technical Digest (online) (Optical Society of America, 2017), paper OM2B.7.

10. Bin Zhang, Angela Davies, John Ziegert, and Christopher Evans "Application of instrument transfer function to a fringe projection system for measuring rough surfaces", Proc. SPIE 10373, Applied Optical Metrology II, 103730S (23 August 2017).

11. Peter de Groot, Xavier Colonna de Lega, Rong Su, and Richard Leach "Does interferometry work? A critical look at the foundations of interferometric surface topography measurement", Proc. SPIE 11102, Applied Optical Metrology III, 111020G (3 September 2019.

12. Richard J. Becherer and George B. Parrent, "Nonlinearity in Optical Imaging Systems*," J. Opt. Soc. Am. 57, 1479-1486 (1967).

13. Orlando ,H., & Thanh, L., “Modulation transfer function (MTF) analysis for a FLIR sustem with nonlinear video electronics”, IEEE (1993).

14. Glenn D. Boreman and Christopher Costanzo "Compensation For Gain Nonuniformity And Nonlinearity In Hgcdte Infrared Charge-Coupled-Device Focal Planes," *Optical Engineering* 26(10), 261081 (1 October 1987).

15. Glenn D. Boreman, Anthony B. Centore, and Christopher R. Costanzo "Spatial harmonic distortion: a test for focal plane nonlinearity," *Optical Engineering* 30(5), (1 May 1991)

16. EdwardW. S. Fry, Sophie Triantaphillidou, Ralph E. Jacobson, Robin B. Jenkin, John R. Jarvis, "Validation of Modulation Transfer Functions and Noise Power Spectra from Natural Scenes.

17. Cecil W. Thomas, "Coherence Function in Noisy Linear System", *International Journal of Biomedical Science and Engineering.* Vol. 3, No. 2, 2015, pp. 25-33.

18. Y. C. Kim, W. F. Wong, E. J. Powers and J. R. Roth, "Extension of the coherence function to quadratic models," in *Proceedings of the IEEE*, vol. 67, no. 3, pp. 428-429, March 1979.

19. G. Carter and C. Knapp, "Coherence and its estimation via the partitioned modified chirp-Z transform," in *IEEE Transactions on Acoustics, Speech, and Signal Processing*, vol. 23, no. 3, pp. 257-264, June 1975.

20. Radoslav Bortel, Pavel Sovka, "Approximation of statistical distribution of magnitude squared coherence estimated with segment overlapping," Signal Processing, Volume 87, Issue 5,2007, Pages 1100-1117, ISSN 0165-1684.

21. B. E. Maki, "Interpretation of the Coherence Function When Using Pseudorandom Inputs to Identify Nonlinear Systems," in *IEEE Transactions on Biomedical Engineering*, vol. BME-33, no. 8, pp. 775-779, Aug. 1986.

22. G. Carter, C. Knapp and A. Nuttall, "Estimation of the magnitude-squared coherence function via overlapped fast Fourier transform processing," in *IEEE Transactions on Audio and Electroacoustics*, vol. 21, no. 4, pp. 337-344.

23. G. C. Carter, "Coherence and time delay estimation," in *Proceedings of the IEEE*, vol. 75, no. 2, pp. 236-255, Feb. 1987.

24. Stein, R. B., French, A. S., & Holden, A. V. (1972). The frequency response, coherence, and information capacity of two neuronal models. *Biophysical journal*, *12*(3), 295–322.

25. Swati Jain, Angela Davies Allen, and Bin Zhang "Evaluation of the spatial frequency response and the uncertainty for a commercial structured light system", Proc. SPIE 11102, Applied Optical Metrology III, 111020X (3 September 2019).

26. Steve Elgar and Vinod Chandran, “Higher order spectral analysis to detect the nonlinear interactions in measured time series and an application to CHUA’s circuit”, International journal of Bifcuraction and chaos, vol. 3, no. (1993), 19-34.

27. Tanbir Ibne Anowar, Gazi Habibul Hyder, Md Jabed Hossain, “Analysis of Higher Order Spectra Compare to Second Order in Digital Signal Processing into the Multi Diversity System and its Applications”, INTERNATIONAL JOURNAL OF ENGINEERING RESEARCH & TECHNOLOGY (IJERT) Volume 02, Issue 12 (December 2013).

28. M. Raghuveer and C. Nikias, "Bispectrum estimation: A parametric approach," in *IEEE Transactions on Acoustics, Speech, and Signal Processing*, vol. 33, no. 5, pp. 1213-1230, October 1985.

29. R. Messina and V. Vittal, "Assessment of nonlinear interaction between nonlinearly coupled modes using higher order spectra," in *IEEE Transactions on Power Systems"*, vol. 20, no. 1, pp. 375-383, Feb. 2005.

30. I. Jouny and R. L. Moses, "The bispectrum of complex signals: definitions and properties," in *IEEE Transactions on Signal Processing*, vol. 40, no. 11.

31. Choudhury S.M., Shah S.L., Thornhill N.F., "Bispectrum and Bicoherence. In: Diagnosis of Process Nonlinearities and Valve Stiction", Advances in Industrial Control. Springer, Berlin, Heidelberg (2008).

32. M. Abolbashari, S.M. Kim, G. Babaie, J. Babaie, F. Farahi, Fractional bispectrum transform definition and properties, IET Signal Process. 11 (2017) 901–908.

33. K. I. Kim and E. J. Powers, "A digital method of modeling quadratically nonlinear systems with a general random input," in *IEEE Transactions on Acoustics, Speech, and Signal Processing*, vol. 36, no. 11, pp. 1758-1769.

34. Y. C. Kim and E. J. Powers, "Digital Bispectral Analysis and Its Applications to Nonlinear Wave Interactions," in IEEE Transactions on Plasma Science, vol. 7, no. 2, pp. 120-131, June 1979, doi: 10.1109/TPS.1979.4317207.Li, S., Liu, Y.: 'Feature Extraction of Lung Sounds Based on BispectrumAnalysis'. Third Int. Symp. on Information Processing, 2010, pp. 393–397

35. Gordon, J.A., Buscher, D.F.: 'Detection noise bias and variance in the power spectrum and bispectrum in optical interferometry', *Astron. Astrophys.*, 2012, 541, p. A46.

36. Silva, Walter A. et al. "Recent Applications of Higher-Order Spectral Analysis to Nonlinear Aeroelastic Phenomena." (2005).

37. Babaie, J. (2019). The fractional bispectrum noise reduction technique and applications in interferometry [published doctoral thesis]. University of North Carolina at Charlotte.

CONCLUSION

A methodology to measure the instrument transfer function (ITF) of a commercial structured light system (the EinScan-Pro 3D Scanner) and the different factors which can contribute to uncertainty have been researched. The importance of the focus condition along with the lateral position of the artifact in field of view has been investigated. The best focus for the EinScan Pro is found to be 380 ± 10 mm and the change in the ITF is negligible within ± 10 mm lateral positioning around the measurement axis. The MTF of each camera was also examined as a function of working distance. The best focus conditions for camera-1 and camera-2 are 390 ± 10 mm. It is observed that both the ITF and the MTF reduce systematically about the best focus condition. A comparison of ITF with MTF shows that the ITF is slightly higher than the MTF at positions closer than best focus and that the ITF is close to the lower MTF of camera-1 for distances beyond best focus. As the literature suggests, we find that the ITF follows the MTF and that the MTF can be used as a reasonable measure of the spatial resolution. The theoretical analysis by Zhang, et al. showed the equivalency of MTF and ITF in the limit that the PSF is small compared to the carrier wavelength [6] and this is the case over the defocus range investigated here. A more rigorous comparison of ITF and MTF would require lower uncertainty ITF measurements.

The second paper includes a discussion of characterizing and validating the step artifact where the step artifact is fabricated from a single-side polished silicon wafer. The implication of the scattering properties of the artifact surface (a diffuse step edge vs. a specular edge) and the dependence of the ITF measurement on the tilt of the step artifact relative to the optical axis of the instrument. A diffuse edge and a specular edge artifact

through experiment and simulation shows the importance of the alignment condition as well as the scattering properties of the artifact. In addition, the influence factors such as the focus condition, position in the measurement volume, step alignment, and various data analysis processing parameters. The sensitivity of the ITF to the step orientation of the artifact within the field of view was also discussed, and the ITF was found to be insensitive to this measurement condition. The choice of the resampling interval was also explored. In addition, the characterization and validation methods for the step artifact were discussed.

The identification test of the non-linearity using the coherence function and the bispectrum was introduced. Both methods were applied to the most commonly used artifacts (sinewave and the step artifact) for MTF and ITF measurements. We show that the bispectrum has the advantage over the coherence function as it can be used for both types of artifacts. Even with a sinewave artifact, for which the coherence function calculation is valid, it is difficult to identify the presence of nonlinearity in the presence of noise. However, the impact of noise is reduced with the bispectrum calculation, improving the ability to detect the nonlinearity. The higher order spectrum calculations could be invested in future work such as the tri-spectrum. The bispectrum is beneficial but the identification of the non-linearity depends on the degree of the non-linearity compared to the noise level present in the signal.

For future work, the fractional bispectrum (FBS) should be investigated as an alternative to the bispectrum. The fractional bispectrum is similar to the bispectrum except that the calculation involves a frequency and a given multiple of the frequency (the fraction), whereas the bispectrum involves a frequency and twice the frequency. In essence the bispectrum is looking at the comparison of each frequency in a step profile compared

to the expected amplitude of 2x that frequency. The amplitude of each *2f* is low compared to the amplitude at *f* for a step artifact, and this reduces the sensitivity of the bispectrum to this nonlinearity check. The fractional bispectrum, on the other hand, can be defined to look at e.g. a frequency *f* and *0.9f*, in which case the amplitudes at both frequencies naturally present in a step artifact are relatively closer (because the two frequencies are closer together), suggesting the impact of nonlinearity on frequency mixing will be more clear. Also, once the nonlinearity has been estimated, approaches to removing the nonlinearity should be explored. Also, the approach described here for measuring the ITF and estimating the uncertainty could be used to then go back to a measurement and improve the resolution (with uncertainty) with a deconvolution operation. Deconvolution approaches are widely used in the field of microscopy.

REFERENCES

1. der Jeught, S. V., and Joris, J. J. D., “Real-time structured light profilometry: a review,” Optics and Laser Enineering 87, 18-31(2016).
2. Gupta, M., Agrawal, A., Veeraraghavan, A. and Narasimhan S.G., “Structured light 3D scanning in presence of global illumination,” Proc. CVPR, 713-720, (2011).
3. Xavier, C. d. L. and de Groot. P. J.,”Lateral resolution and instrument transfer function as criteria for selecting surfave metrology instruments,” Imaging and Applied Optics Technical Digest, OTu1D4, (2012).
4. de Groot, P., Lega, X. C. De., de Lega, X. C., “Interpreting interferometric height measurements using the instrument transfer function,” Fringe 2005, 30–37, Springer Berlin Heidelberg, Berlin, Heidelberg (2006).
5. Zhang,B. , D. Allen,A., Ziegert, J. and Evans, C., “Validity of the instrument transfer function for fringe projection metrology,” Applied optics, Vol 57, No. 11, 2795-2803 (2018)
6. Zhang,B. , D. Allen,A., Ziegert, J. and Evans, C., “Application of instru- ment transfer function to a fringe projection system for measuring rough surfaces,” Proc. SPIE 10373, 103730S (2017).
7. Berssenbrügge, P., Dekiff, M., Kemper, B., Denz, C.., Dirksen, D., “Characterization of the 3D resolution of topometric sensors based on fringe and speckle pattern projection by a 3D transfer function,” Opt. Lasers Eng. **50**(3), 465–472 (2012).
8. Kellner, T., Breitbarth, A., Zhang, C. and Notni, G., “Characterizing 3D sensors using the 3D modulation transfer function,” Measurement Science and Technology, 29,1-8 (2018).

9. Leach, R., Giusca, C., Henning, A., Sherlock, B. and Coupland, J., “ISO definition of resolution for surface topography measuring instruments,”, Fringe, 405-410 (2013).

10. Tianquan Su, Alejandro Maldonado, Peng Su, and James H. Burge, "Instrument transfer function of slope measuring deflectometry systems," Appl. Opt. 54, 2981-2990 (2015).

11. Torsten Glaschke, Leslie L. Deck, and Peter J. de Groot "Characterizing the resolving power of laser Fizeau interferometers", Proc. SPIE 10829, Fifth European Seminar on Precision Optics Manufacturing, 1082905 (7 August 2018).

12. Daniel M. Sykora and Peter de Groot, "Instantaneous measurement Fizeau interferometer with high spatial resolution", Proc. SPIE 8126, Optical Manufacturing and Testing IX, 812610 (27 September 2011).

13. L. L. Deck and P. J. de Groot, "Using the instrument transfer function to evaluate Fizeau interferometer performance," in *Optical Design and Fabrication 2017 (Freeform, IODC, OFT)*, OSA Technical Digest (online) (Optical Society of America, 2017), paper OM2B.7.

14. Peter de Groot, Xavier Colonna de Lega, Rong Su, and Richard Leach "Does interferometry work? A critical look at the foundations of interferometric surface topography measurement", Proc. SPIE 11102, Applied Optical Metrology III, 111020G (3 September 2019.

15. Richard J. Becherer and George B. Parrent, "Nonlinearity in Optical Imaging Systems*," J. Opt. Soc. Am. 57, 1479-1486 (1967).